
**High-latitude Precipitation:
characterizing snowfall regimes and
identifying key processes at two
distinct Scandinavian sites**

Julia A. SHATES

A thesis submitted in partial fulfillment of
the requirements for the degree of
(Atmospheric and Oceanic Sciences)

at the

UNIVERSITY OF WISCONSIN-MADISON

2019

Abstract

High-latitude Precipitation: characterizing snowfall regimes and identifying key processes at two distinct Scandinavian sites

by Julia A. SHATES

In the Arctic and subarctic, the challenges of studying snowfall are exacerbated by a scarcity of observations and harsh conditions. Microphysical properties of snowfall in the high-latitudes such as ice habit, particle size distribution, and the effects of riming, impact larger scale processes occurring over ice sheets and mountain snowpack. However, the future of high latitude precipitation patterns is uncertain. Amplified warming in the Arctic and implied changes to the hydrologic cycle make it critical to understand snowfall. This study utilizes a new and unique data set from ground-based in-situ and remote sensing instrumentation at two distinct sites in Scandinavia collected as part of the NSF-funded High-Latitude Measurement of Snowfall (HiLaMS) project to investigate and define snowfall regimes in the high-latitude winter months (November-April). The links between meteorological conditions, snowfall characteristics, and the regional environment in Haukelisetser, Norway and Kiruna, Sweden are studied using observations from: a ground-based, K-band, vertically-pointing Micro Rain Radar (MRR), and surface-based meteorological measurements. Hourly ERA5 reanalysis products provide insight to the associated synoptic scale conditions, while radar profile information is used to infer properties of distinct snowfall cases that are dominated by wind speed, wind direction, and surface temperature. By defining the meteorological context for the snowfall regimes, a better understanding is developed on the conditions that govern these precipitation processes and how they differ at these two sites.

Dedicated to my grandparents, Olga and Michael Umansky.

Acknowledgements

Thank you to Dr. Tristan L'Ecuyer and Dr. Claire Pettersen for advising and mentoring me, and for sharing your enthusiasm in researching snowfall.

Thank you to Dr. Jonathan Martin and Dr. Steve Vavrus for your thoughtful feedback on my project.

Thank you to my peers, friends, and members of the AOS department (faculty and staff) that have helped me navigate graduate school.

Thank you to my family who have encouraged me to take on new challenges, and to explore Wisconsin.

Thank you to my twin sister, Tessa Shates. Thank you for believing in me, being excited for me... and giving me edits on very rough, rough drafts.

Thank you to my partner, James Winkelman. Thank you for being here to uplift me and support me in reaching for my goals. Also, thank you for listening to all of my practice presentations over and over again.

Contents

| | |
|--|------------|
| Dedication | ii |
| Acknowledgements | iii |
| Contents | iv |
| List of Figures | vi |
| List of Tables | xii |
| 1 Introduction | 1 |
| 1.1 Preface | 1 |
| 1.1.1 Hydrologic Cycle | 2 |
| 1.1.2 Energy Balance | 4 |
| 1.1.3 Challenges and Methods in Observing Snowfall | 5 |
| 1.1.3.1 Ground-based Radar | 6 |
| 1.1.3.2 Spaced-based Observations | 7 |
| 1.1.3.3 Instrument suites | 8 |
| 1.1.4 Snowfall at two distinct Scandinavian sites | 9 |
| 1.1.5 Introduction Figures | 10 |
| 2 Site, Instrumentation, Data | 16 |
| 2.0.1 Site description | 16 |
| 2.0.2 Instrumentation | 17 |
| 2.0.3 Reanalysis Data | 20 |
| 2.0.4 Tables and Figures | 20 |
| 3 Methods | 26 |
| 3.0.1 Precipitation Occurrence and Events | 26 |
| 3.0.1.1 Precipitation occurrence for winter analysis | 27 |
| 3.0.1.2 Precipitation events | 27 |
| 3.0.2 Methods Figures | 28 |

| | | |
|----------|---|-----------|
| 4 | Results | 32 |
| 4.0.1 | Climatological Conditions | 32 |
| 4.0.2 | Precipitation Occurrence | 34 |
| 4.0.3 | Regimes/Representative Cases | 36 |
| 4.0.3.1 | Haukeliseter Deep snowfall | 36 |
| 4.0.3.2 | Haukeliseter Shallow snowfall | 38 |
| 4.0.3.3 | Haukeliseter Intermittent/Pulsed Snowfall | 39 |
| 4.0.3.4 | Kiruna Deep Snowfall | 41 |
| 4.0.3.5 | Kiruna Shallow Snowfall | 43 |
| 4.0.3.6 | Kiruna Intermittent Snowfall | 44 |
| 4.0.3.7 | Snow Virga | 45 |
| 4.0.4 | Results Figures | 46 |
| 5 | Discussion and Synthesis | 70 |
| 6 | Conclusions | 75 |
| 6.1 | Conclusions and Future Directions | 75 |
| | Bibliography | 79 |

List of Figures

| | | |
|-----|---|----|
| 1.1 | Figure 1 from Bintanja and Andry (2017) of changes in Arctic snowfall fraction for RCP8.5 forcing. a Present day (2006-2015). b Future (2091-2100). c Twenty-first Century trend, defined as absolute difference between future and present-day snowfall fractions. Stippling denotes regions where the difference is not significant. | 11 |
| 1.2 | Figure 1 from Instanes et al. (2016) of Hydropower installations in the Arctic | 12 |
| 1.3 | Top: Figure from Rasmussen et al. (2012) of hydropower stations in the Arctic. Bottom: Liquid Water Equivalent Accumulation of snowfall from three different sensors at Haukeliseter, Norway. Two precipitation gauges shielded by a single fence, third precipitation gauge shielded by a double wind fence. | 13 |
| 1.4 | Figure 1 from Devasthale and Norin (2014) of 12 C-band radars in Swedish weather radar network. Areas enclosed by red circles used for analysis . . | 14 |
| 1.5 | Figure from Kulie et al. (2016) of snowfall fraction from CloudSat observations of shallow cumuliform clouds and nimbostratus clouds for 2006-2010. a shallow cumuliform snowfall fraction, b nimbostratus snowfall fraction | 15 |
| 2.1 | Top: Google earth image over Northern Scandinavia with location marker on Kiruna, Sweden. Bottom: Google earth image over south-western Norway with location marker over Haukeliseter, Norway | 21 |
| 2.2 | Map with site locations and ERA5 coordinates | 22 |
| 2.3 | Figure of Northern Hemisphere storm track density from Hoskins and Hodges (2002) from tracking negative, cyclonic mean sea level pressure features | 23 |
| 2.4 | Photo of the MRR at the site in Kiruna, Sweden. Courtesy of Steven J. Cooper | 24 |
| 2.5 | Photo of the weather instruments at the Haukeliseter site including the Double Fence, one of the single fences, and the tower with the wind and temperature measurements. Courtesy of Claire Pettersen. | 25 |
| 3.1 | Schematic of methods flow for precipitation occurrence and for precipitation events | 29 |
| 3.2 | Radar Reflectivity for Oct 2017 0000-1200UTC in Kiruna, Sweden. Vertical lines mark the hours that are flagged positive for precipitation | 30 |

| | | |
|-----|---|----|
| 3.3 | Research flow chart used to characterize and describe the precipitation events | 30 |
| 3.4 | 2D histogram of Radar Reflectivity (Z_e) [dBz] for snowfall case on 4 November 2017 in Haukeliseter, Norway. Color-bar & values represent bin count normalized with the total number of observations. Y axis: height above ground level (AGL) and X axis: Z_e | 31 |
| 4.1 | Box & Whisker plot for mean monthly temperature distributions at sites for winter months (November-April) 1979-2018. The horizontal dashed lines represent the mean temperature of the month for the entire climatological period. The boxes span the interquartile range and the whiskers show the highest and lowest value (excluding outliers). The mean monthly temperature during months of the deployments are superimposed as black stars onto the respective boxes. | 47 |
| 4.2 | Box & Whisker plots of monthly distributions from surface temperature observations and ERA5 2m temperature for the months during winter months (November-April) in 2016-2017 in Haukeliseter and 2017-2018 in Kiruna. The left column figures are for distributions in Haukeliseter and the right are for Kiruna, Sweden. The upper figures are for the temperature distribution of the full month; the bottom figures are temperature distributions during precipitation events. | 48 |
| 4.3 | Windroses of the winter climatology at each site of ERA5 10m winds. The climatological winter period is for November-April from 1979 to 2018. Left: winter winds in Haukeliseter. Right: winter winds in Kiruna. Colors represent wind speed in units of ms^{-1} . The quadrant provides information on the source direction and the size of the rose shows the frequency. . . . | 49 |
| 4.4 | Windroses of monthly distributions of surface wind observations and ERA5 10m winds during winter months (November-April) in 2016-2017 in Haukeliseter and 2017-2018 in Kiruna. Colors represent wind speed in units of ms^{-1} . The left column figures are for distributions in Haukeliseter and the right are for Kiruna, Sweden. The upper figures are for the winds from surface observations; the bottom figures are the 10m winds from ERA5 reanalyses. | 50 |
| 4.5 | Windroses during precipitation of monthly distributions of surface wind observations and ERA5 10m winds in the winter months (November - April) in 2016-2017 in Haukeliseter and 2017-2018 in Kiruna. The left column figures are for distributions in Haukeliseter and the right are for Kiruna, Sweden. The upper figures are for the winds from surface observations; the bottom figures are the 10m winds from ERA5 reanalyses. | 51 |
| 4.6 | Radar profiles during deep snowfall event in Haukeliseter, Norway from 4 November 2016 (0157 UTC) - 6 November 2016 (0236 UTC). Left: time x height profile of radar reflectivity (Z_e). Right: time x height profile of Doppler Velocity (V_d). | 52 |

| | | |
|------|---|----|
| 4.7 | Left: 2D histogram of Ze; Center: 2D histogram of Vd; Right: 2D histogram of σ . Color-bar & values represent bin count normalized with the total number of observations | 52 |
| 4.8 | Synoptic & Climatological context of a given hour during snowfall event: 5 November 2016 0500 UTC. For synoptic context (left): mean sea level pressure (msl) in mb is in the shading and 500mb geopotential height (z500) contours are overlayed. Climatological context (right): msl anomaly in shading and z500 black line contours; negative z500 anomalies are dashed. | 53 |
| 4.9 | Meteorological Surface Observations. Left: 10m winds during event. Right: Temperature observations during event smoothed with 15 minute running mean. | 53 |
| 4.10 | Average vertical Profiles of temperature and relative humidity from ECMWF ERA5 reanalyses during event. Left: Temperature & dashed line at 2°C indicates temperature threshold between snow and rain; Right: Relative humidity & dashed line is 100% relative humidity with respect to water. Shading represents range between average profile and standard deviation below and above | 54 |
| 4.11 | Left: ERA5 10m winds during event (0200UTC - 1300UTC). Right: Meteorological Surface Temperature observations during event | 54 |
| 4.12 | Radar profiles during shallow snowfall event in Haukeliseter, Norway from 6 February 2017 (0158 UTC) - 7 February 2017 (1315 UTC). Left: time x height profile of radar reflectivity (Ze). Right: time x height profile of Doppler Velocity (Vd). | 55 |
| 4.13 | Left: 2D histogram of Ze; Center: 2D histogram of Vd; Right: 2D histogram of σ . Color-bar & values represent bin count normalized with the total number of observations | 55 |
| 4.14 | Synoptic & Climatological context of a given hour during snowfall event: 7 February 2017 0700 UTC. For synoptic context (left): mean sea level pressure (msl) in mb is in the shading and 500mb geopotential height (z500) contours are overlayed. Climatological context (right): msl anomaly in shading and z500 black line contours; negative z500 anomalies are dashed. | 56 |
| 4.15 | Average vertical profiles of temperature and relative humidity from ECMWF ERA5 reanalyses during event. Left: Temperature & dashed line at 2°C indicates temperature threshold between snow and rain; Right: Relative humidity & dashed line is 100% relative humidity with respect to water. Shading represents range between average profile and standard deviation below and above | 56 |
| 4.16 | Meteorological Surface Observations. Left: 10m winds during event. Right: Temperature observations during event smoothed with 15 minute running mean. | 57 |

| | | |
|------|---|----|
| 4.17 | Radar profiles during shallow snowfall event in Haukeliseter, Norway from 21 December 2016 (0626 UTC) - 26 December 2016 (1714 UTC). Left: time x height profile of radar reflectivity (Z_e). Right: time x height profile of Doppler Velocity (V_d). | 57 |
| 4.18 | Zoomed in to the first 16 hours of the Intermittent/Pulsed event in Haukeliseter on 21 December, 2016. Left: profile of radar reflectivity. Right: Profile of Doppler Velocity. | 58 |
| 4.19 | Left: 2D histogram of Z_e ; Center: 2D histogram of V_d ; Right: 2D histogram of σ . Color-bar & values represent bin count normalized with the total number of observations | 58 |
| 4.20 | Synoptic & Climatological context of a given hour during snowfall event: 23 February 2017 2300 UTC. For synoptic context (left): mean sea level pressure (msl) in mb is in the shading and 500mb geopotential height (z_{500}) contours are overlayed. Climatological context (right): msl anomaly in shading and z_{500} black line contours; negative z_{500} anomalies are dashed. | 59 |
| 4.21 | Average vertical profiles of temperature and relative humidity from ECMWF ERA5 reanalyses during event. Left: Temperature & dashed line at 2°C indicates temperature threshold between snow and rain; Right: Relative humidity & dashed line is 100% relative humidity with respect to water. Shading represents range between average profile and standard deviation below and above | 59 |
| 4.22 | Radar profiles during shallow snowfall event in Kiruna, Sweden from 5 November 2017 (01436 UTC) - 5 November 2017 (11:07 UTC). Left: time x height profile of radar reflectivity (Z_e). Right: time x height profile of Doppler Velocity (V_d). | 60 |
| 4.23 | Left: 2D histogram of Z_e ; Center: 2D histogram of V_d ; Right: 2D histogram of σ . Color-bar & values represent bin count normalized with the total number of observations | 60 |
| 4.24 | Meteorological Surface Observations. Left: 10m winds during event. Right: Temperature and relative humidity observations during event smoothed with 15 minute running mean. | 61 |
| 4.25 | Synoptic & Climatological context of a given hour during snowfall event: 6 November 2017 0000 UTC. For synoptic context (left): mean sea level pressure (msl) in mb is in the shading and 500mb geopotential height (z_{500}) contours are overlayed. Climatological context (right): msl anomaly in shading and z_{500} black line contours; negative z_{500} anomalies are dashed. | 61 |
| 4.26 | Average vertical profiles of temperature and relative humidity from ECMWF ERA5 reanalyses during event. Left: Temperature & dashed line at 2°C indicates temperature threshold between snow and rain; Right: Relative humidity & dashed line is 100% relative humidity with respect to water. Shading represents range between average profile and standard deviation below and above | 62 |

| | | |
|------|---|----|
| 4.27 | Meteorological Surface Observations. Left: 10m winds during event. Right: Temperature and relative humidity observations during event smoothed with 15 minute running mean. | 62 |
| 4.28 | Radar profiles during shallow snowfall event in Kiruna, Sweden from 17 February 2018 (01459 UTC) - 19 February 2018 (0722 UTC). Left: time x height profile of radar reflectivity (Ze). Right: time x height profile of Doppler Velocity (Vd). | 63 |
| 4.29 | Left: 2D histogram of Ze; Center: 2D histogram of Vd; Right: 2D histogram of σ . Color-bar & values represent bin count normalized with the total number of observations | 63 |
| 4.30 | Synoptic & Climatological context of a given hour during snowfall event: 18 February 2018 1100 UTC. For synoptic context (left): mean sea level pressure (msl) in mb is in the shading and 500mb geopotential height (z500) contours are overlayed. Climatological context (right): msl anomaly in shading and z500 black line contours; negative z500 anomalies are dashed. | 64 |
| 4.31 | Average vertical profiles of temperature and relative humidity from ECMWF ERA5 reanalyses during event. Left: Temperature & dashed line at 2°C indicates temperature threshold between snow and rain; Right: Relative humidity & dashed line is 100% relative humidity with respect to water. Shading represents range between average profile and standard deviation below and above | 64 |
| 4.32 | Meteorological Surface Observations. Left: 10m winds during event. Right: Temperature and relative humidity observations during event smoothed with 15 minute running mean. | 65 |
| 4.33 | Radar profiles during shallow snowfall event in Haukelisetser, Norway from 21 December 2016 (0626 UTC) - 26 December 2016 (1714 UTC). Left: time x height profile of radar reflectivity. Right: time x height profile of Doppler Velocity (Vd). | 65 |
| 4.34 | Left: 2D histogram of Ze; Center: 2D histogram of Vd; Right: 2D histogram of σ . Color-bar & values represent bin count normalized with the total number of observations | 66 |
| 4.35 | Synoptic & Climatological context of a given hour during snowfall event: 8 December 2017 0900 UTC. For synoptic context (left): mean sea level pressure (msl) in mb is in the shading and 500mb geopotential height (z500) contours are overlayed. Climatological context (right): msl anomaly in shading and z500 black line contours; negative z500 anomalies are dashed. | 66 |
| 4.36 | Average vertical profiles of temperature and relative humidity from ECMWF ERA5 reanalyses during event. Left: Temperature & dashed line at 2°C indicates temperature threshold between snow and rain; Right: Relative humidity & dashed line is 100% relative humidity with respect to water. Shading represents range between average profile and standard deviation below and above | 67 |

| | | |
|------|---|----|
| 4.37 | Meteorological Surface Observations. Left: 10m winds during event. Right: Temperature and relative humidity observations during event | 67 |
| 4.38 | Radar profiles during shallow snowfall event in Haukeliseter, Norway from 1 December 2017 (1343 UTC) - 1 December 2017 (1659 UTC). Left: time x height profile of radar reflectivity (Z_e). Right: time x height profile of Doppler Velocity (V_d). | 68 |
| 4.39 | Left: 2D histogram of Z_e ; Center: 2D histogram of V_d ; Right: 2D histogram of σ . Color-bar & values represent bin count normalized with the total number of observations | 68 |
| 4.40 | Synoptic & Climatological context of a given hour during snowfall event: 1 December 2017 1500 UTC. For synoptic context (left): mean sea level pressure (msl) in mb is in the shading and 500mb geopotential height (z_{500}) contours are overlaid. Climatological context (right): msl anomaly in shading and z_{500} black line contours; negative z_{500} anomalies are dashed. | 69 |
| 4.41 | Average vertical profiles of temperature and relative humidity from ECMWF ERA5 reanalyses during event. Left: Temperature & dashed line at 2°C indicates temperature threshold between snow and rain; Right: Relative humidity & dashed line is 100% relative humidity with respect to water. Shading represents range between average profile and standard deviation below and above | 69 |

List of Tables

| | | |
|-----|---|----|
| 2.1 | Summarized site information: instruments deployed at the sites and variables used in this study | 22 |
| 5.1 | Summary table of snowfall regimes/representative cases at the two Scandinavian sites | 72 |

Chapter 1

Introduction

1.1 Preface

From tiny snow crystals to the growth of ice sheets, high-latitude snowfall is important within the climate system and society. At local, regional and global scales snowfall is a direct driver of the hydrologic cycle and energy balance (Vihma et al., 2016). For society, snowfall is important for water resources and hydropower (Instanes et al., 2016). However, it remains a challenge to observe and measure snowfall. In the high-latitudes, observations are scarce (Vihma et al., 2016), and this is exacerbated by the challenges in measuring snowfall (Rasmussen et al., 2012, Wolff et al., 2015). Also, in forecasts and modeling, snowfall is one of the most difficult variables to simulate; the models represent snow as its liquid equivalent, but the actual snow reaching the surface and accumulating depth has to be determined by a ratio between the snow and its liquid equivalent (Ware

et al., 2006). In addition to challenges in predicting snow on day-to-day timescales, the long term future of snowfall is uncertain because of global warming (Collins et al., 2013); especially in the high-latitudes where surface temperatures are warming faster than the rest of the world (Serreze and Barry, 2011). However, the changes are not projected to be the same across the high-latitudes. Regions such as the Barents and Kara seas stand out in particular with a future trend showing a decline in snowfall and increase in rainfall (see bottom plot in Fig. 1.1 from Bintanja and Andry (2017)). This chapter motivates the need to study snowfall by providing context of the role of snow in the changing climate and in society.

1.1.1 Hydrologic Cycle

Snowfall is the main source in the surface mass balance (SMB) of glaciers and ice sheets, and accumulation of mountain snowpack (Souverijns et al., 2018, Stewart, 2009). The properties of the snow impacts how much accumulates in terms of its depth and liquid water equivalent. The snow density depends on structure/habit of the ice crystals (Ware et al., 2006), which is a function of the temperature and moisture in the atmosphere (Libbrecht, 2005). Across the snowy Northern Hemisphere, regions such as the Greenland Ice Sheet (GrIS) and high elevation mountains are impacted by these snowfall properties. Over the GrIS, distinct snowfall regimes identified by Pettersen et al. (2018) contribute differently to accumulation. Fully glaciated clouds and clouds containing cloud liquid water produced different amounts of snowfall at the surface and did not occur with the same frequency. Also they were found to coincide with specific atmospheric circulation

patterns. Some studies show that atmospheric circulation patterns will shift as a response to global warming (Liu et al., 2012), and alter the hydrologic cycle. Liu et al. (2012) attribute anomalously large amounts of winter snow over the Northern United States, northwestern and central Europe, and northern and central China to low autumn Arctic sea ice.

In mountainous regions, accumulation of snow is linked to water resources and hydropower. The amount and timing of snowfall directly impacts the snowpack and snow cover over a region (Stewart, 2009). Extreme precipitation events, such as those associated with atmospheric rivers, contribute to large amounts of snowpack accumulation in regions such as the Sierra Nevada Mountains on the Western coast of the United States (Guan et al., 2010), and streamflow from snowmelt is important for water supply in many regions the Northern Hemisphere (Stewart, 2009). In Nordic countries, especially Norway and Sweden, hydropower from snowpack is integral for the nations' electricity. Instanes et al. (2016) describe Scandinavia's use of hydropower: Norway's domestic electricity generation from hydropower is 94% and Sweden's is 65%. Figure 1.2 illustrates the large number of medium sized hydropower plants across Scandinavia, which reinforces the importance of snowfall in this region for electricity and water resources. Hydropower generation is closely tied to their economies; prices of electricity fluctuate based on whether it's a dry or wet year. During dry years, the Nordic nations must rely more heavily on other (more expensive) resources for electricity (Instanes et al., 2016).

Precipitation also affects high-latitude ecosystems. There are an increasing number of observed rain-on-snow (ROS) events attributed to the warming winter surface temperatures (Vikhamar-Schuler et al., 2016), which impacts the ability of animals to feed. It has been observed in Scandinavia that ROS events lead to a refrozen layer within the snowpack that reindeer are unable to break through to reach food resources (Putkonen and Roe, 2003). The properties of precipitation such as phase and how much accumulates directly impact these animals, which can in turn impact the people who depend on them.

1.1.2 Energy Balance

Snowfall emits and scatters radiation (Skofronick-Jackson et al., 2015), and on local and regional scales, accumulated snow impacts the surface energy balance (SEB) (Lund et al., 2017). Through their field study over varying surfaces on the GrIS, Lund et al. (2017) determined the impact of snow cover on the SEB of dry tundra, wet tundra and ice. Their study illustrates that the presence of snow decreased the spatial heterogeneity and the SEB variation among the different sites. Winters with low snowfall have an impact on the SEB the following spring, particularly in dry tundra. These drier winters decrease the contribution of the latent heat flux and increase the sensible heat flux observed the following spring.

At the global scale, the bright, snow-covered arctic surface reflects incoming solar radiation back out to space and decreases the heat absorbed by the sun (Serreze and Barry, 2011). The extent of snow cover and the duration controls the amount of shortwave radiation absorbed, and terrestrial snow cover impacts the climate system (Vavrus, 2007).

In a modeling study, Vavrus (2007) shows that snow cover is necessary for the formation of extremely cold air outbreaks in the high-latitudes. In addition, the study shows that the lack of terrestrial snow cover leaves the surface exposed to cold air and freezes the soil, which may play an important role in permafrost feed-backs and climate change.

The microphysical properties - specifically the phase- of precipitation can also potentially have large consequences for the earth's energy budget in the changing climate. The albedo of dry snow over sea ice is higher than other land, ice and snow surfaces (Perovich et al., 2002). Just as terrestrial snow reflects sunlight back to space, loss of sea ice contributes to the positive sea ice-albedo feedback accelerating global warming and climate changes. Screen and Simmonds (2012) observe that a decline in summer snowfall, corresponding to an increase in the rainfall, impacts the sea ice. At the site in the Canadian Arctic, there was a decrease in sea ice albedo as a result of the rainfall on the ice (Screen and Simmonds, 2012). This result suggests changes in precipitation phase can reinforce climate feedbacks.

1.1.3 Challenges and Methods in Observing Snowfall

As mentioned earlier, there are relatively few observations in the high-latitudes (Vikhamar-Schuler et al., 2016), and where there are observation platforms, it is difficult for instrumentation to measure solid precipitation (Rasmussen et al., 2012, Wolff et al., 2015). Compared to rain, snow is extremely sensitive to wind and turbulence, and blowing snow and instrument under-catch are common issues in the snowy Arctic and Antarctic (Rasmussen et al., 2012, Souverijns et al., 2018). Precipitation gauges need to be modified to account for the impacts of wind; for example, wind shields and fences decrease the

wind speed around a gauge and improve the amount captured (Rasmussen et al., 2012, Wolff et al., 2015). The top panel in Fig. 1.3 from Rasmussen et al. (2012) shows a simple schematic of a double wind fence/shield around a precipitation gauge, and illustrates wind vectors decreasing near the instrument. Wolff et al. (2015) observe the effects of wind on snowfall in the mountainous region of Haukeliseter, Norway, and their site contains two single fenced sensors and a Double Fence Intercomparison Reference (DFIR)/Double Fence Automatic Reference (DFAR). The bottom panel in Fig. 1.3 shows the liquid water equivalent (LWE) accumulation of snowfall from the two single fences and the DFIR at Haukeliseter on 22 December 2016. In total LWE for 24 hours, the DFIR measures nearly 25mm while the single fences measure substantially less LWE (10mm and 5mm, respectively). In addition to wind-related challenges, instruments, such as profiling radars, require more power for heating to avoid snow accumulation on top of the radar dish (Maahn et al., 2012).

1.1.3.1 Ground-based Radar

Where available, ground-based scanning radar networks are useful for weather forecasting and studying snowfall in high-latitudes. Figure 1.4 shows the locations of C-band scanning radars that are part of the Swedish weather radar network used in studies from Devasthale and Norin (2014), Norin et al. (2015, 2017). Norin et al. (2017) determined the sensitivity of snowfall to eight distinct weather states: four wind directions, the two phases of the North Atlantic Oscillation (NAO), and positive/negative mean sea level

pressure over the region. They showed that the effects of larger scale circulation patterns interacting with local meteorology and topography affect the intensity of snowfall. However, Norin et al. (2015, 2017) point out limitations of the ground-based network: when the snow is occurring further away from the radar, the radar beam can completely overshoot precipitation. The red circles around each radar in Fig. 1.4 indicate the area/range surrounding the radars that were determined reliable for precipitation analyses. Ground-based scanning radars are limited by their inability to detect shallow precipitation and have a limited range surrounding the sites. Also, terrain and mountains interfere with the radar signal (Smalley et al., 2014).

1.1.3.2 Spaced-based Observations

Satellite observations have also been used to study snowfall in the high-latitudes. For example, Skofronick-Jackson et al. (2015) combine spaced-based observations from active and passive sensors with ground-based and airborne measurements to study falling snow during the Global Precipitation Measurement Cold Season Precipitation Experiment (GCPEX), over Ontario, Canada. Norin et al. (2015) also explore space-based observations by comparing snowfall vertical profiles observed by the W-band cloud radar on CloudSat to the ground-based Swedish weather radar network. Kulie et al. (2016) use CloudSat observations to characterize global snowfall by analyzing the vertical profiles. Kulie et al. (2016) show the existence of distinct snowfall regimes from the vertical radar profiles: shallow cumuliform primarily over oceans and nimbostratus over land (see

Fig. 1.5). While satellites improve the accessibility of studying remote high-latitude regions, the space-based sensors are unable to completely observe shallow snowfall (Norin et al., 2015). For active sensors, ground clutter makes the lower 1km to 1.5km above the ground unusable (Kulie et al., 2016, Norin et al., 2015).

1.1.3.3 Instrument suites

At high-latitude sites, there has been recent success using ground-based vertically profiling radars to infer characteristics about snowfall. Souverijns et al. (2018) and Gorodetskaya et al. (2015) study snowfall and surface mass balance of the Antarctic ice sheet using a vertically profiling radar in combination with a suite of ground-based instruments at Princess Elizabeth station in Antarctica. They show that large snowfall accumulation occurs with atmospheric river events that reach the frozen continent and bring moisture from lower latitude sources. Schirle et al. (2019) studied snowfall and improved snow retrievals using observations from a suite of instruments and the same type of vertically profiling radar at a mountainous site in southern Norway. Consistent with the work using the Swedish weather radar network (Devasthale and Norin, 2014, Norin et al., 2017), they show that the wind direction impacts snowfall due to the topography in the region. Similarly, Pettersen et al. (2018) linked snowfall to cloud type and the atmospheric circulation over GrIS using a suite of remote sensing instruments. Back trajectory analysis showed that snow events associated with clouds containing cloud liquid water occur when air masses slowly advect from the south and south-west, but snow events from fully

glaciated clouds originate from the North Atlantic side of Greenland and quickly move across the GrIS. (Pettersen et al., 2018).

1.1.4 Snowfall at two distinct Scandinavian sites

The results from these snowfall studies motivate further questions about high-latitude precipitation. Specifically, this study is focused on the influence of topography and large-scale circulation on snowfall and how they may lead to distinct snowfall regimes. The methods combine weather observations, various ground-based remote sensing instruments, and climate reanalyses to explore snowfall characteristics. We use observations from a vertically profiling radar to better understand the snowfall regimes occurring over two sites in Scandinavia. By using climate reanalyses to study the synoptic scale context associated with snowfall events, we connect the the local scale radar observations to the larger circulation. This document is organized into separate sections and all figures are at the end of their respective sections. In Chapter 2, the sites, instrumentation and reanalysis data are described. Then in Chapter 3, the methods used to study climatological conditions at the sites, conditions during precipitation, and the properties of the precipitation are explained. The results are in Chapter 4, and the discussion and synthesis are in Chapter 5. Chapter 6 contains conclusions and future directions.

This study focuses on the following questions to guide the characterization and exploration of high-latitude snowfall in Scandinavia. Through these questions we hope to gain a better understanding of the processes affecting precipitation occurring locally and how they're connected to environment and the larger scale atmospheric conditions. And through

these observations and analyses, we can develop a stronger base of knowledge on areas in precipitation microphysics and precipitation in the climate system that could potentially be applied to snowfall forecasting and understanding/modeling changes in precipitation in a warming climate.

The study questions are:

1. How are snowfall events influenced by their environment? How do synoptic scale weather patterns and topography influence the type of snowfall in a region? Can we identify the physical mechanisms influencing distinct snowfall regimes?

2. How do snowfall regimes vary across distinct regions in the high latitudes? How are snowfall patterns and physical mechanisms unique to those areas?

1.1.5 Introduction Figures

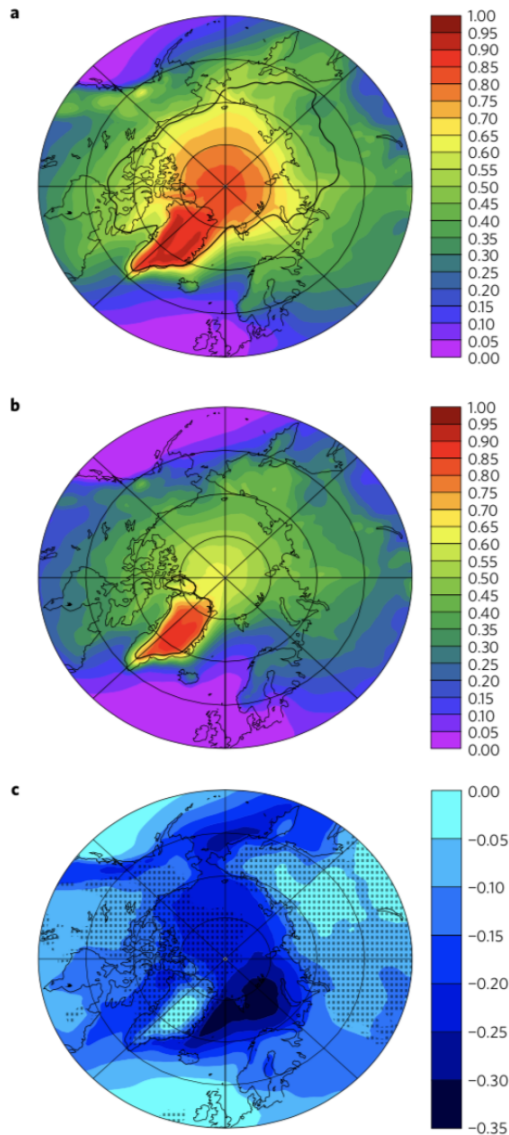


FIGURE 1.1: Figure 1 from Bintanja and Andry (2017) of changes in Arctic snowfall fraction for RCP8.5 forcing. **a** Present day (2006-2015). **b** Future (2091-2100). **c** Twenty-first Century trend, defined as absolute difference between future and present-day snowfall fractions. Stippling denotes regions where the difference is not significant.



FIGURE 1.2: Figure 1 from Instanes et al. (2016) of Hydropower installations in the Arctic

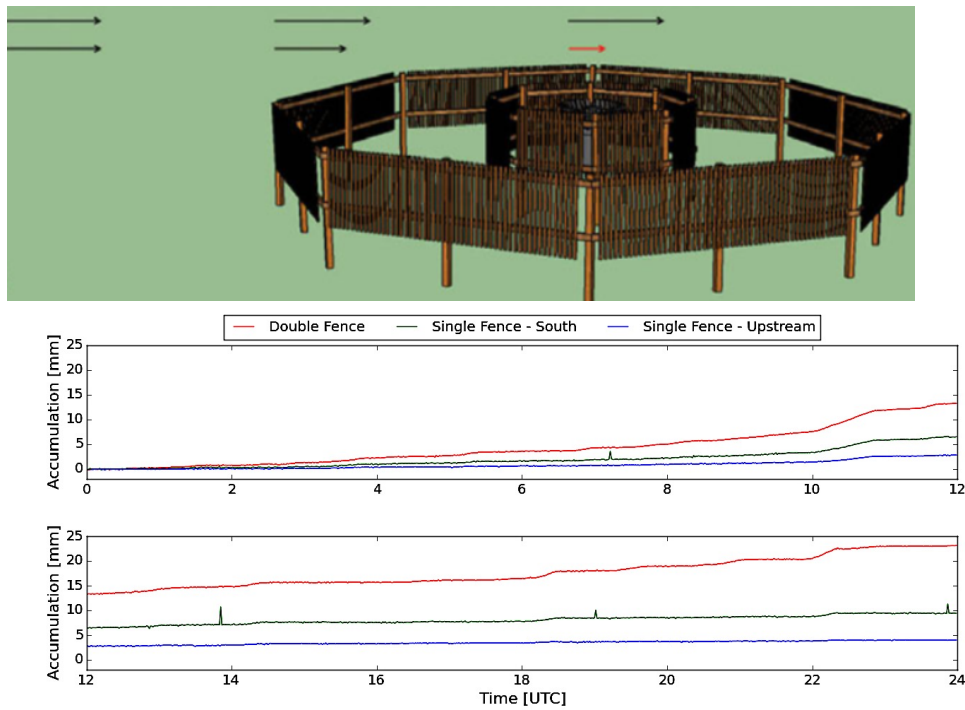


FIGURE 1.3: Top: Figure from Rasmussen et al. (2012) of hydropower stations in the Arctic. Bottom: Liquid Water Equivalent Accumulation of snowfall from three different sensors at Haukeliseter, Norway. Two precipitation gauges shielded by a single fence, third precipitation gauge shielded by a double wind fence.

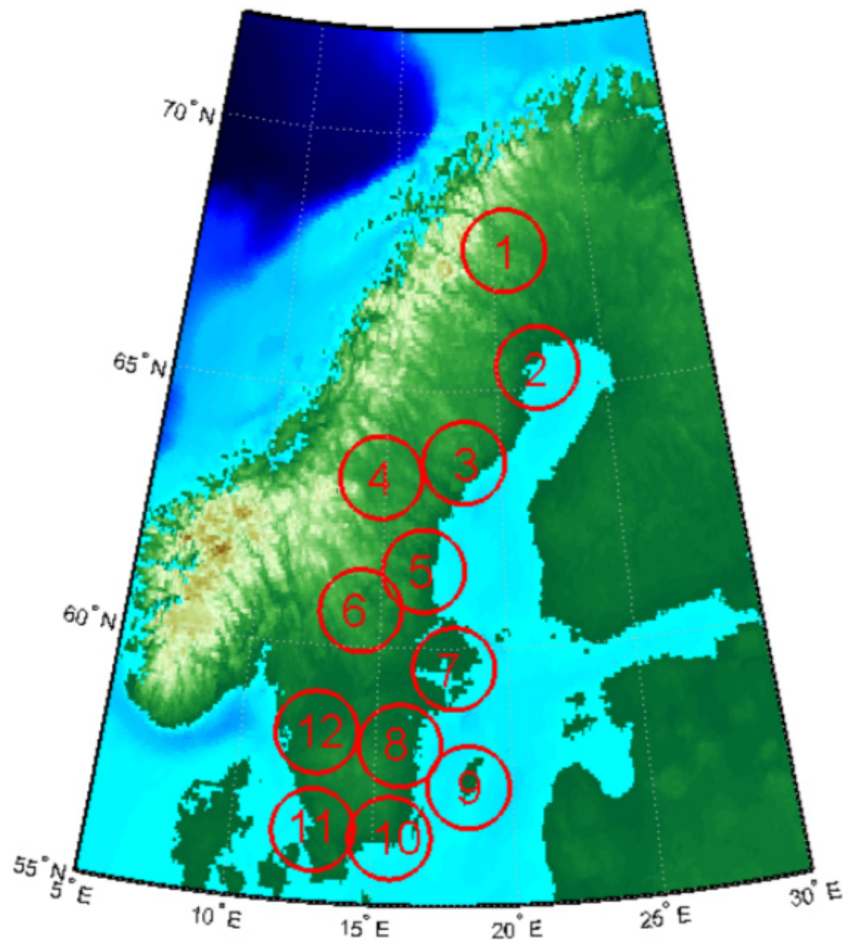


FIGURE 1.4: Figure 1 from Devasthale and Norin (2014) of 12 C-band radars in Swedish weather radar network. Areas enclosed by red circles used for analysis

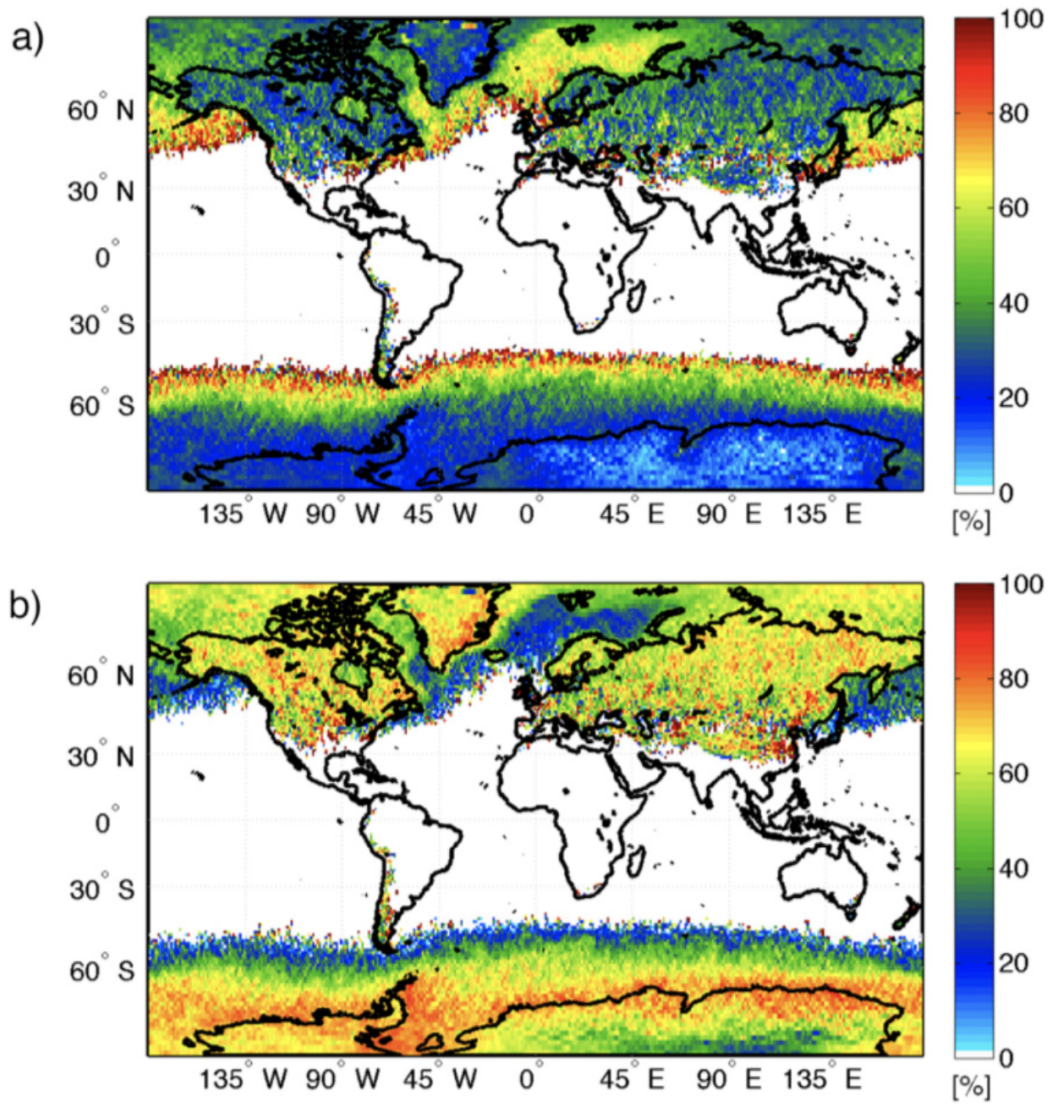


FIGURE 1.5: Figure from Kulie et al. (2016) of snowfall fraction from CloudSat observations of shallow cumuliform clouds and nimbostratus clouds for 2006-2010. **a** shallow cumuliform snowfall fraction, **b** nimbostratus snowfall fraction

Chapter 2

Site, Instrumentation, Data

2.0.1 Site description

The Scandinavian peninsula is a high-latitude stretch of land from approximately 55°N to 70°N with varying topography across the region. There are mountains, fjords along the coast, mountain fjords, proglacial lakes (see Fig. 2.1), and areas of discontinuous and sporadic regions of permafrost (Gisnås et al., 2017). It is relatively warm for its high-latitude position due to ocean heat transport from the Gulf Stream and interactions with the atmospheric circulation (Seager et al., 2002). Figure 2.3 from Hoskins and Hodges (2002) shows the storm track density over the Northern Hemisphere given in units of 10^6km^2 per month; and the track density can be defined as the number of systems passing through a grid box per unit area. Over the North Atlantic region and across Scandinavia, and through the Barents and Kara Seas, the track density is high; this indicates that

this region experiences frequent extra-tropical storms. In addition, extreme precipitation events such as atmospheric rivers (ARs), or moisture intrusions from lower latitudes, interact with the topography on the Scandinavian peninsula (Sodemann and Stohl, 2013).

This work explores snowfall at two Scandinavian sites: Haukeliseter, Norway and Kiruna, Sweden (see Fig. 2.2). Haukeliseter, Norway (59.81°N , 7.21°E , 991m) is a sub-arctic site in the mountainous southwest region of Norway. It is less than 150km from the western coast, and between the coast and the summit site, the terrain includes steep mountain fjords changing from sea level to the peaks over 990m. Southeast of the site, the topography includes a gentle, increasing slope towards the summit. The region experiences high wind speeds and snowfall in the winter and months outside of meteorological winter (Wolff et al, 2014). Approximately 1000 km away, the second site is at Kiruna, Sweden (67.84°N , 20.41°E , 530m). This northern Nordic site is within the Arctic circle and is drier, colder and has lower wind speeds than at Haukeliseter. The topography west and southwest of Kiruna includes the Kebnekaise mountain range which includes the highest peak in Sweden. Also, the terrain surrounding the site includes areas of permafrost, and proglacial and kettle lakes.

2.0.2 Instrumentation

For each winter season at the respective sites, there were ground-based instruments deployed. Table 2.1 summarizes the instruments and variables. We define winter as November-April. Both sites had a METEK Micro Rain Radar 2 (MRR) (pictured in

Figure 2.4), which is a vertically profiling 24GHz (K-band) frequency-modulated, continuous wave Doppler radar (Klugmann et al, 1996). This small and portable radar was originally developed for observing precipitation on buoys in the North Sea, and is not sensitive to sea spray or clouds. The Maahn and Kollias (2012) method for processing the Doppler spectra of the MRR precipitation profile is used to obtain the effective radar reflectivity (Z_e) in decibels (dBz), Doppler velocity (V_d) in ms^{-1} and spectrum width (σ) in ms^{-1} for snowfall at a one-minute time resolution. While the MRR is able to profile up to 3km above ground level (AGL), precipitation above this height is undetected. Data below 300m AGL are removed due to the effects of ground clutter on the measurements; precipitation is considered to reach the surface when it is observed at 300m AGL.

The effective radar reflectivity is sensitive to the number, size and density/mass of the particles. Some precipitation types are related to typical radar reflectivity ranges; values below 0dBz indicate weak/ light precipitation, 0-10dBz is associated with drizzle or light snow, the 10-30dBz range generally indicates heavy snow or rain, and values above 30dBz include melting snow and heavy rain (Houze Jr, 2014, p. 112). The Doppler velocity provides a measure of the motion of the air combined with the velocity of particles moving toward or away from the radar. Positive Doppler velocity values indicate that the particles and motion of the air are toward the radar. Negative values mean that the motion is away from the radar and can be indicative of turbulence in the column. The spectrum width provides a measure of the dispersion of particle motions (Rinehart, 1991, p. 127). The Doppler spectra from the vertical profile makes it possible to study snowfall characteristics and the mechanisms/processes taking place as snow forms above the radar

(Matrosov et al., 2008). The Doppler velocity and the spectrum width provide qualitative information on the riming and turbulence in the precipitation column (Matrosov et al., 2008). Mitchell et al. (1990) observed that rimed snow particles during snowfall events in the Sierra Nevada Mountains had more mass as opposed to aggregates. This suggests that processes occurring at the microphysical level are tied to larger scale issues such as the amount of snow water equivalent (SWE)/liquid equivalent stored in mountain snowpack.

Weather data were provided by the Norwegian Meteorological Institute for the site in Haukeliseter, Norway, (pictured in Figure 2.5), and the Luleå University of Technology provided observations from Kiruna, Sweden. The observations include wind speed and direction (10m AGL at Haukeliseter, 2m AGL at Kiruna), surface temperature and relative humidity (RH). At Haukeliseter, the snow accumulation is measured as Liquid Water Equivalent (LWE) from a Geonor precipitation gauge shielded by a double wind fence (DFIR) (Wolff et al., 2015). For accumulation in Kiruna, we calculate the LWE from the Doppler spectra using a Ze-S relationship (equation 2.1) for dry snowfall (Matrosov, 2007) that was modified by Kneifel et al. (2011). We use the radar reflectivity at 400m AGL to calculate the snowfall rate.

$$Ze = 56 * S^{1.2} \tag{2.1}$$

2.0.3 Reanalysis Data

Reanalysis data provide climatological context at the sites and synoptic scale context during precipitation events. The winter climatological time period is 1979-2018 for November-April. The European Centre for Medium-Range Weather Forecasts (ECMWF) ERA5 data are on a $.25^\circ \times .25^\circ$ spatial grid resolution (30km), and the temporal resolution is hourly (<https://www.ecmwf.int/en/forecasts/datasets/reanalysis-datasets/era5>). The spatial resolution improves at the higher latitudes. By using the (2.2), the calculated grid resolution is 19km at Haukeliseter and 17km at Kiruna. Figure 2.2 shows the site coordinates on the map and the ERA5 coordinates are superimposed to verify their proximity. The ERA5 coordinates are: $60^\circ\text{N}/7.25^\circ\text{E}$ for Haukeliseter, Norway; and $68^\circ\text{N}/20.5^\circ\text{E}$ for Kiruna, Sweden. The variables we include in our analyses are: 500mb geopotential height, mean sea level pressure (msl), 2m temperature (surface temperature), 10m v and u components of wind (surface winds), and vertical profiles of temperature and relative humidity.

$$Area_{gridbox} = 2 * \pi * R_{earth}^2 * | \sin(lat1) - \sin(lat2) | | lon1 - lon2 | / 360^\circ \quad (2.2)$$

2.0.4 Tables and Figures

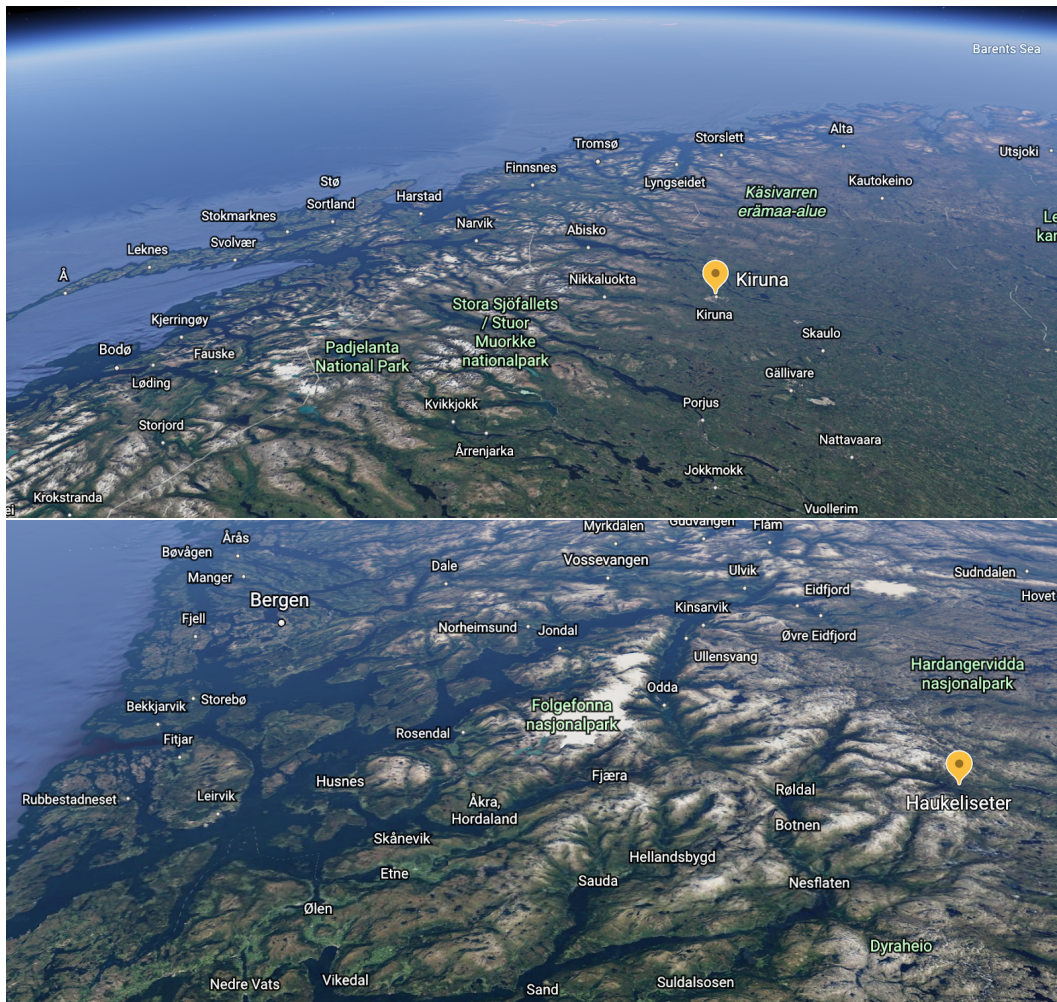


FIGURE 2.1: Top: Google earth image over Northern Scandinavia with location marker on Kiruna, Sweden. Bottom: Google earth image over south-western Norway with location marker over Haukeliseter, Norway

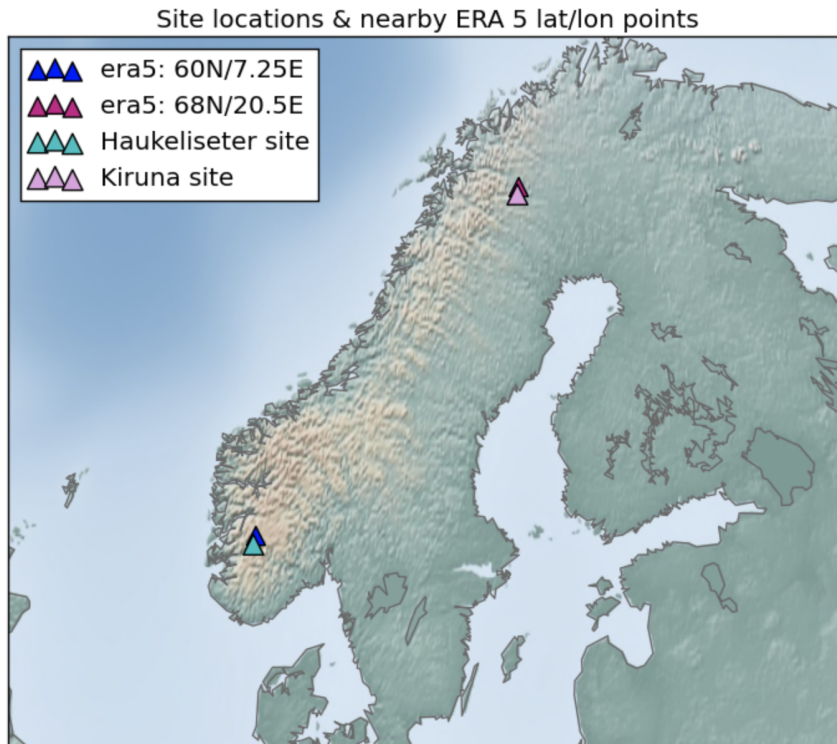


FIGURE 2.2: Map with site locations and ERA5 coordinates

| Instruments & site information | |
|--|---|
| Haukeliseter, Norway 59.81N, 7.21E, 991m | Kiruna, Sweden 67.84N, 20.41E, 530m |
| October-June, 2016-2017 | September-May, 2017-2018 |
| Micro Rain Radar 2: Radar Reflectivity, Doppler Velocity, spectrum Width | Micro Rain Radar 2: Radar Reflectivity, Doppler Velocity, spectrum Width |
| Weather station: 10m winds, temperature, Double Fence snow accumulation | Weather station: 2m winds, temperature, relative humidity |
| Particle Imaging Package (PIP): particle size distributions, particle fallspeeds | Particle Imaging Package (PIP): particle size distributions, particle fallspeeds |
| Multi Angle Snow Camera (MASC): high resolution images of snowflakes, particle fallspeeds | Dual Ice Crystal Imaging (D-ICI) Probe: high resolution images of snowflakes |

TABLE 2.1: Summarized site information: instruments deployed at the sites and variables used in this study

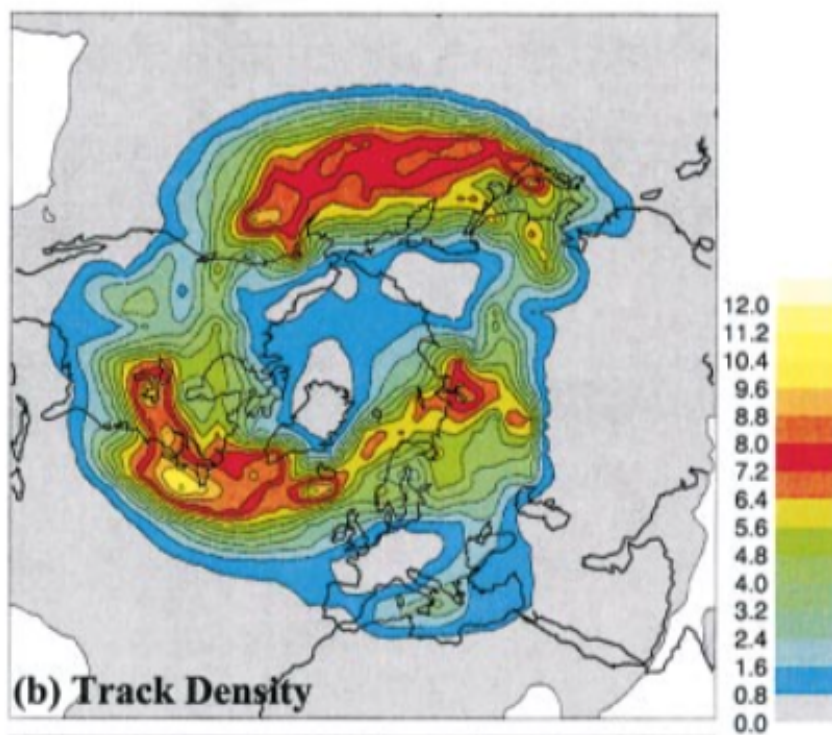


FIGURE 2.3: Figure of Northern Hemisphere storm track density from Hoskins and Hodges (2002) from tracking negative, cyclonic mean sea level pressure features



FIGURE 2.4: Photo of the MRR at the site in Kiruna, Sweden. Courtesy of Steven J. Cooper



FIGURE 2.5: Photo of the weather instruments at the Haukeliseter site including the Double Fence, one of the single fences, and the tower with the wind and temperature measurements. Courtesy of Claire Pettersen.

Chapter 3

Methods

3.0.1 Precipitation Occurrence and Events

The following section outlines methods to analyze the winter season precipitation and to explore precipitation events at each respective site. The chart in Fig. 3.1 illustrates a general flow for the methods. First, we are interested in conditions when the MRR identifies precipitation during winter months; a threshold in radar reflectivity of -10dBz is applied to the data. Then the chart branches off to two separate analyses: precipitation occurrence and precipitation events. For precipitation occurrence, the focus is on comparing winds and temperature in climatological time period to winds and temperature during deployment months. Precipitation events are identified separately and we use case studies. The surface temperature provides a rough distinction between solid and liquid precipitation; temperatures less (greater) than 2°C suggest solid (liquid).

3.0.1.1 Precipitation occurrence for winter analysis

Precipitation flags are used to combine the hourly resolution reanalyses with the one-minute resolution radar data. An hour is flagged as precipitating if 10 minutes of radar reflectivity values are greater than or equal to -10dBz within the 15 minutes before and after each hour (10min/30min). Figure 3.2 depicts when an hour is flagged as precipitating in an example case at the Kiruna, Sweden site. This example also shows that precipitation can occur on very short time scales; by using a 10 minute threshold, we focus on data that are representative of the conditions around the hour.

3.0.1.2 Precipitation events

Events are separated by a minimum of 6 hours between the last detected hydrometeor and the first detected hydrometeor of the following event. Then, an additional threshold must be reached: the event must last at least 3 hours between the initial and final detection. In contrast to precipitation occurrence, the events include gaps/time between radar echos. In the previous section, the focus is on conditions when there is precipitation. Here, by including gap times, we are interested in how the event may evolve, and whether the precipitation is continuous or intermittent. We manually selected precipitation cases to analyze based on their radar profiles. We chose cases that have defining features/structures in their profiles, and cases that appear with some frequency during the winter deployment that qualitatively represent the snowfall regimes at the sites.

For each event, we are interested in characterizing the snowfall and their unique properties. The flow chart in Fig. 3.3 outlines specific questions used to explore the properties. The flow begins with radar observations, then meteorological surface observations, and we use the ERA5 reanalyses to determine the synoptic scale context associated with the snowfall events.

We analyze the radar profiles using time series of the observations and 2D histograms for the events. Using the 2D histogram allows us to remove/compress the time dimension and summarize the radar profile of the event. Figure 3.4 contains an example of the 2D histogram for one of the snowfall cases from the results in Chapter 4. The color in the histogram represents normalized bin count while the axes are height above ground level (AGL) and radar reflectivity in dBz. Areas with large normalized bin counts indicate higher observations at that height for that reflectivity value. Changes throughout the column such as an increase of radar reflectivity with decreasing height can suggest that there are more particles near the surface or larger/more massive particles; additional information from the thermodynamic profile and surface meteorology can then indicate what kind of physical processes are occurring, such as riming or aggregation.

3.0.2 Methods Figures

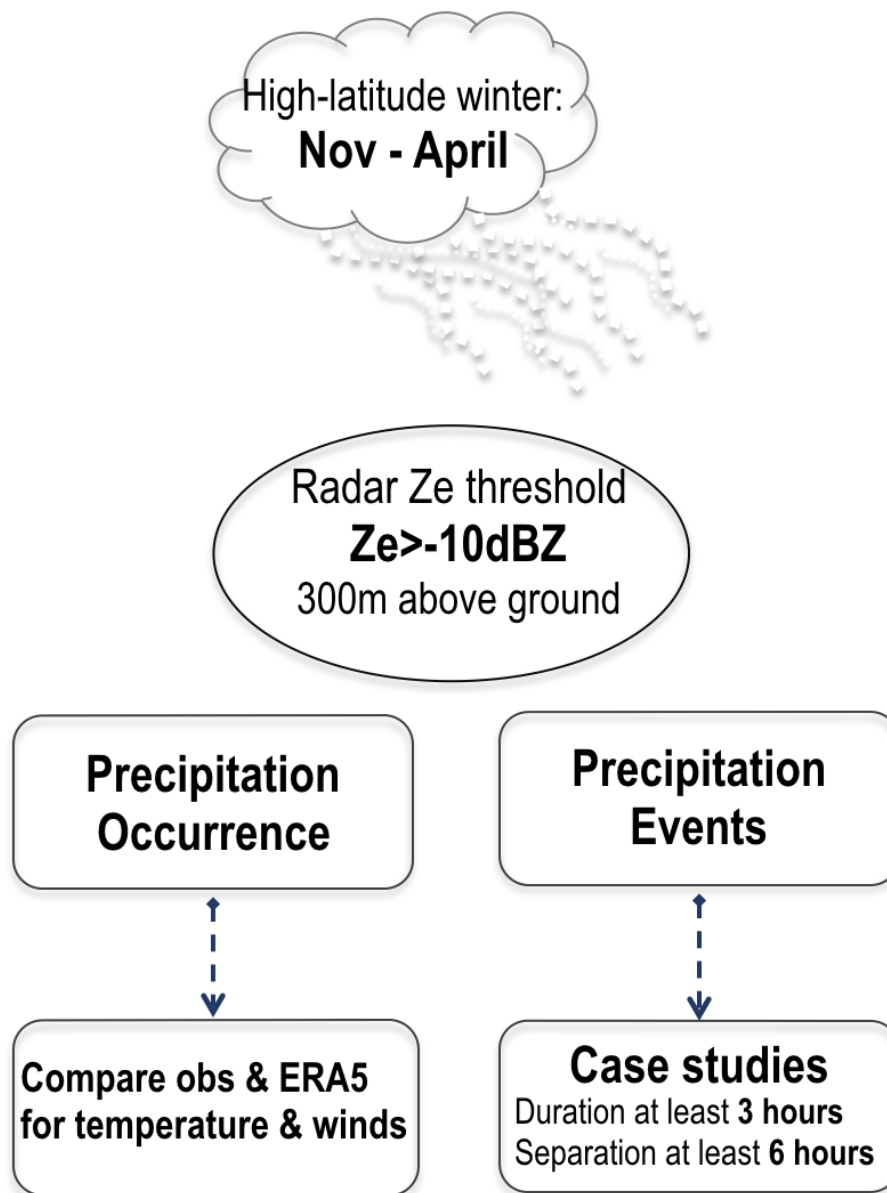


FIGURE 3.1: Schematic of methods flow for precipitation occurrence and for precipitation events

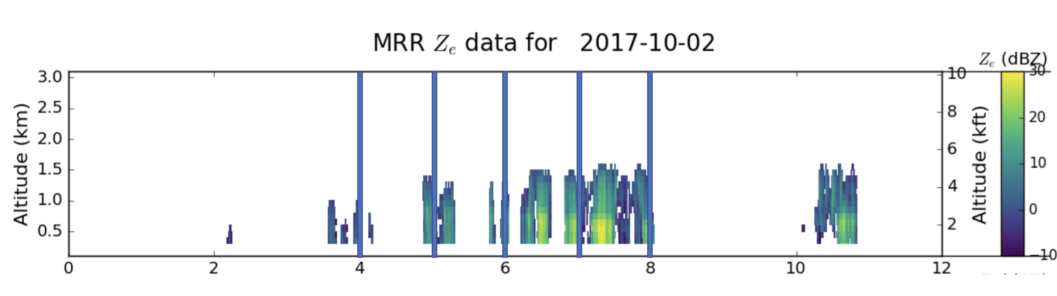


FIGURE 3.2: Radar Reflectivity for Oct 2017 0000-1200UTC in Kiruna, Sweden. Vertical lines mark the hours that are flagged positive for precipitation

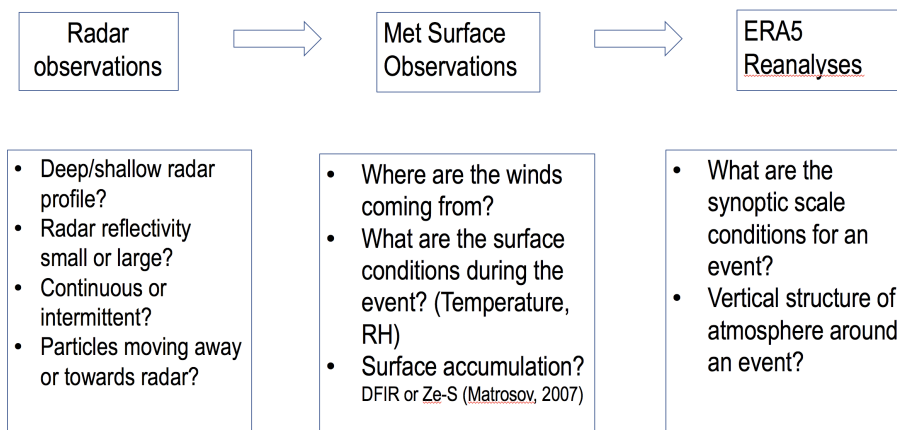


FIGURE 3.3: Research flow chart used to characterize and describe the precipitation events

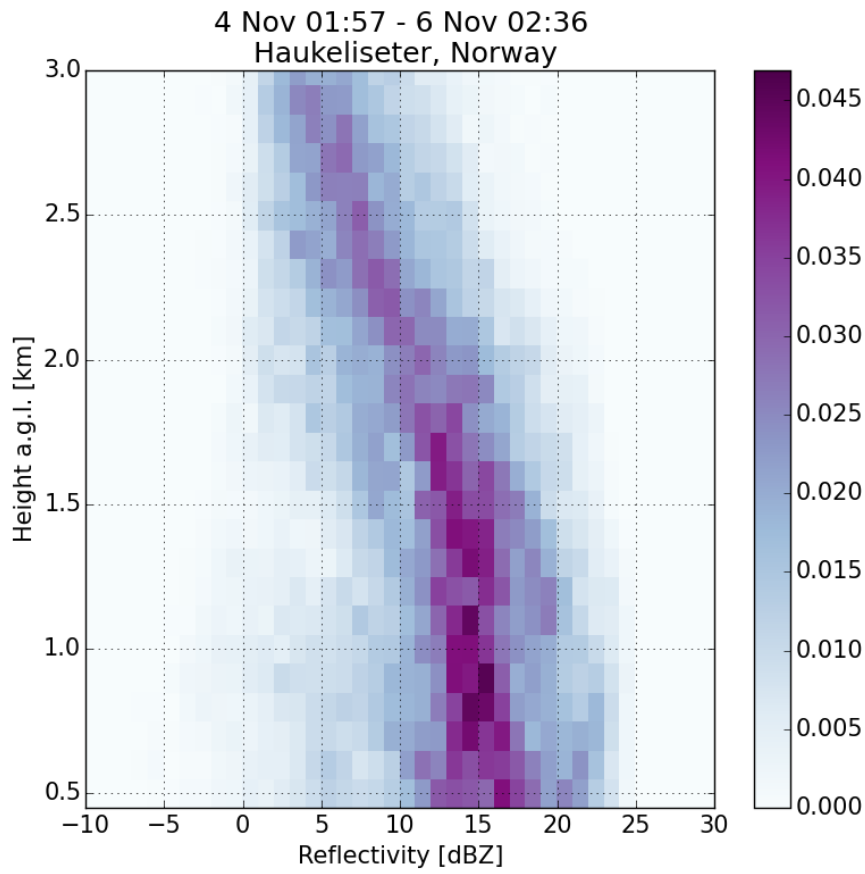


FIGURE 3.4: 2D histogram of Radar Reflectivity (Z_e) [dBZ] for snowfall case on 4 November 2017 in Haukeliseter, Norway. Color-bar & values represent bin count normalized with the total number of observations. Y axis: height above ground level (AGL) and X axis: Z_e

Chapter 4

Results

During the winter months November-April, there are 55 distinct events identified in Haukeliseter during 2016-2017, and 59 in Kiruna during 2017-2018. There are three general regimes (or representative cases) exhibited in Haukeliseter: deep, shallow, and intermittent/pulsed; and four general regimes in Kiruna: deep, shallow, intermittent, and snow virga.

4.0.1 Climatological Conditions

This section describes the temperature and wind conditions at the sites for winter months in 1979-2018, and the conditions during months of deployment. The winter climatology of surface temperatures for Haukeliseter, Norway and Kiruna, Sweden are shown in the box and whisker plot in Fig. 4.1. The winter months in Kiruna are colder than in Haukeliseter, but there is also a larger spread in the Kiruna temperature extremes, especially in

the coldest months of DJF. April is an exception in that the temperature range in Kiruna reaches warmer values than in Haukelisetter. Both sites are dominated by below freezing temperatures between November and April, but the warm extremes show that temperatures can exceed 5°C in Haukelisetter, even in DJF. During the respective deployments, the mean monthly temperatures fell within the interquartile range of the climatologies, except for December 2016 at Haukelisetter where the mean temperature was warmer than the upper quartile range. The warmer than average temperatures were even recognized by local news sources that commented that the December weather was as warm as summer in Norway (Local, 2016).

The top panel in Fig. 4.2 shows how the box and whiskers compare in the surface observations and the ERA5 surface temperatures. In Haukelisetter (left), the ERA5 surface temperatures were colder than the surface observations at the site for all the months excluding February where the ERA5 mean temperature was warmer. The temperature distribution in Kiruna (right) displays the opposite pattern: the mean temperatures were colder in the ground-observations than in the ERA5, with the exception of April.

The windroses in Figs. 4.3 and 4.4 illustrate the winds by their direction, speed, and frequency at Haukelisetter and Kiruna. The windroses in Fig. 4.3 show the climatological (ERA5, winter 1979-2019) surface winds at Haukelisetter (left windrose) and Kiruna (right windrose). The dominant wind directions shown in the winter climatology for both sites are westerly and south-westerly. Kiruna also has a substantial portion of winds coming from the south. The winds represented in this ERA5 climatology are relatively light with

values between 1 and 3ms^{-1} , and in Haukeliseter, a small fraction of wind speeds range from 3 to 5ms^{-1} . The top panel in Fig. 4.4 shows the wind surface observations at the sites during the respective winter deployments. Westerly winds still dominate, but in Haukeliseter (left windrose), the winds are more north-westerly and the speeds are higher with observations exceeding 15ms^{-1} . Also, a small fraction of winds are from the south-east with lower wind speeds than the westerly and north-westerly winds. In Kiruna (right rose), south-westerly winds are still the dominant wind direction in the winter, but a large fraction of winds was also detected from the north and south-east. Wind speeds were mostly 1 to 3ms^{-1} , but some south-westerly winds were measured between 5 and 7ms^{-1} . The ERA5 windroses during the respective winter deployment months are shown in the bottom panel in Fig. 4.4. The wind direction for Haukeliseter (left) qualitatively match the surface observations, but the speeds are lower than the ground-based measurements. For Kiruna, the wind speeds are relatively well represented (mostly 1 to 3ms^{-1} and 5 to 7ms^{-1}), but the wind directions are poorly represented as the fraction of south-westerly winds is too small and the fraction of north-westerly winds is much larger than in the surface measurements.

4.0.2 Precipitation Occurrence

This section reviews conditions associated with winter precipitation over the sites. The bottom panel of box and whisker plots in Fig. 4.2 illustrate temperature distributions during precipitation. In general, the range in temperature values are more narrow at

both sites. In Kiruna (right), the temperatures indicate that the precipitation was primarily snowfall from November-March. In April, the temperatures suggest the occurrence of snowfall and rainfall within a relatively narrow range between -4°C and 5°C . In Haukeliseter (left), the temperatures during precipitation contained warm values in the distribution throughout the winter, with the exception of February where precipitation coincided with only cold temperatures.

The winds during precipitation events are shown in Fig. 4.5. In Haukeliseter (Fig. 4.5 upper left), the winds are dominated by two main wind modes: strong westerly winds, and moderate south-easterly winds. The westerly winds are the most common, accounting for over 50% of the precipitation occurrence, and reach speeds of 15 ms^{-1} and higher. Over 26% of the winds associated with precipitation are from the south-east and are slower in comparison with speeds ranging $7\text{-}9\text{ ms}^{-1}$. The windrose of surface observations in Kiruna (upper right) illustrates that during precipitation, there are two dominant wind modes: 24% northerly and over 46% south-easterly. A small fraction of winds (8%) also come from the south, south-west direction. The south-easterly winds occur the most frequently with speeds between 1 and 5 ms^{-1} . While the northerly occur less frequently, they have higher wind speeds. The south-westerly winds occur with the least frequency, but have the highest speeds reaching $7\text{-}9\text{ ms}^{-1}$.

The bottom panel in Fig. 4.5 displays the ERA5 representation of surface winds when precipitation is occurring. For Haukeliseter (bottom left), the reanalyses have the westerly wind mode, but the the south-easterly winds are poorly represented. Also, the westerly

winds are slower and the highest values range between 7 and 9ms^{-1} . The Kiruna winds (bottom right) are better represented in the ERA5 reanalyses. The south-easterly and northerly winds are included, but the small fraction of south-westerly winds are completely missing.

4.0.3 Regimes/Representative Cases

This section contains descriptions of the events at Haukeliseter and Kiruna. The descriptions include characteristics of the radar profiles, surface meteorological conditions, the synoptic scale context, and the vertical profiles of temperature and RH.

4.0.3.1 Haukeliseter Deep snowfall

The MRR detected the start of a deep snowfall event in Haukeliseter, Norway at 0157 UTC on 4 November 2016. After 48.6 hours, the DFIR measured 23.86mm of LWE accumulation. The precipitation is continuous throughout the event and the profile extends to 3km height (see Fig. 4.6). Schirle et al. (2019) identified this snowfall event as an upslope event; where the south-easterly winds indicate that the air moved over a gradual slope towards the site. In the left panel of Fig. 4.7, the 2D histogram of radar reflectivity shows that this deep, continuous precipitation also has a defined and narrow structure of increasing and broadening radar reflectivity with decreasing height. The reflectivity values near the surface range from approximately 5dBz to 24dBz. The 2D histogram of Doppler velocity (center panel in Fig. 4.7) shows that the velocities are primarily positive

and the motion is near 1ms^{-1} , but ranges from $.75\text{ms}^{-1}$ to 1.25ms^{-1} at lower heights. The spectrum width (right panel in Fig. 4.7), broadens from 0.25ms^{-1} to greater than $.25$, and then greater than 0.5ms^{-1} with decreasing height. The increasing reflectivity with decreasing height suggests that the particles may be aggregating and/or riming- both processes would alter the reflectivity of the particle. The broad and large Doppler velocity values supports riming in the column. Also, Schirle et al. (2019) identify particle riming during this snowfall event through snowflake imagery from a Multi-Angle Snowflake Camera (MASC) at the site.

The synoptic conditions associated with the deep snowfall are characterized by a weak low pressure system developing south of Norway over the North Sea extending over the site (see Fig. 4.8 left). In Fig. 4.8 (right), there is anomalous high pressure north of the region across the Norwegian Sea, most of the Scandinavian peninsula, and Barents Sea. Anomalous low pressure and geopotential heights correspond to the location of the weak low pressure system in the North Sea. The vertical profile of the RH (see Fig. 4.10 right) shows that there was moistening through the boundary layer and free atmosphere. The temperature profile in Fig. 4.10 (left) varies little throughout this 48 hours. The temperature below 900mb is warmer than -10°C , and the relatively warm values approaching 0°C reinforces the likelihood of snowflakes riming and/or aggregating together in the column; riming of super-cooled liquid water and snowflakes aggregating occur at temperatures near the melting point (Houze Jr, 2014, p. 150). At the surface, the temperature is relatively warm near -5°C until it dips down below -7° at the end of the event (see Fig. 4.9). The south-easterly wind direction (windrose in Fig. 4.9) combined

with the synoptic context suggests the North Sea is a local moisture source for this deep snowfall event.

4.0.3.2 Haukeliseter Shallow snowfall

On February 6th 2017, there was a shallow snowfall event that started at 0158 UTC and lasted approximately 35.28 hours. The winds were from the south-east and the temperatures dropped from -6°C to -14°C (Fig. 4.11). The DFIR accumulation was unavailable for this event, but from the Ze-S relationship, the Doppler derived LWE accumulation was 4.28mm. The precipitation appears continuous and is shallow with most observations of precipitation below 1.5km (see Fig. 4.12). The 2D histogram of radar reflectivity in the center panel of Fig. 4.13 shows that the reflectivity values are broad and range from -5dBz to 10dBz, but some observations reach as high as 15dBz. The 2D histogram of Doppler velocity (see center in Fig. 4.13) shows that within the shallow snowfall column there is a broad range of motions from -1ms^{-1} to 2ms^{-1} . The spectrum width is also high with values above $.5\text{ms}^{-1}$ (see right panel in Fig. 4.13) and reinforces that the shallow column was turbulent with updrafts and large spread in particle motions and potentially sizes.

The map of mean sea level pressure and 500mb geopotential heights (left panel in Fig. 4.14) indicates that there was a strong high pressure over the Scandinavian region during this shallow snowfall event. These conditions persisted throughout the event (not shown); this snowfall event occurred under a persistent, strong high pressure system. For the

month of February, the mean sea level pressure was anomalously high (right panel in Fig. 4.14). In combination with the south-easterly winds, this synoptic set-up suggests cold air advected from the cold Eurasian Continent. The vertical structure of the atmosphere (Fig. 4.15) during this shallow snowfall has a strong temperature inversion, and the RH profile shows that the moisture is contained within the shallow boundary layer capped by the stable temperature structure.

4.0.3.3 Haukeliseter Intermittent/Pulsed Snowfall

The MRR detected a high-impact, intermittent/pulsed snowfall event starting at 0626 UTC on 21 December 2016. Measurements indicate there were strong winds (see windrose in Fig. 4.16) and large accumulation - 117.78 mm LWE- over the course of approximately 130.8 hours. The surface meteorological measurements show that the event was relatively warm and near 0°C for most of the time, with temperatures above 2°C at the end of the event (see Fig. 4.16). The precipitation is deep (reaching 3km) and appears intermittent in the radar (Fig. 4.17); there are periods of very high reflectivity interrupted by observations with very low reflectivity or no hydrometeors detected at all. The 2D histogram in the left panel of Fig. 4.19 shows that there is a broad spread in the reflectivity values from 0dBz to values exceeding 25dBz. The Doppler velocity values (center panel in Fig. 4.19) indicate upward vertical air/particle motions and updrafts ranging from 0 to -1ms^{-1} . By zooming into the first 6 hours (1000 minutes) of the event, the extreme variations between the values of the radar reflectivity and Doppler velocity during the event stand out (see

Fig. 4.18). The spread in particle motions falling towards (and away from) the radar is large and increases near the surface where the spectrum width values surpass 1.5ms^{-1} (see right panel in Fig. 4.19). Combined with the large upward motions in the Doppler velocity, the high spectrum width values indicate turbulence within the column. Because of the warmer temperatures at the surface and the vertical motions, it is possible that riming may be occurring which increases the mass of the solid precipitation and would therefore increase the observed radar reflectivity. The local effects of orography enhance the intermittent precipitation, and as the Doppler velocity switches between upward and downward motions, the intermittent precipitation is also pulsed.

This large precipitation event occurred with three separate and consecutive deep low pressure systems. The geopotential height contours show a defined trough bringing the storms to the coast (see left panel of figure 4.20). Throughout the extended period of deep low pressure systems over the region, the vertical profile of RH in the right panel of Fig. 4.21 shows that the atmosphere is moist through the boundary layer and free atmosphere. The vertical profile of temperature also confirms the warm temperatures (greater than 0°C) in the lower levels of the atmosphere (left panel in Fig. 4.21). The low pressure system nearest to 26 December was named Extreme Storm Urd and reached hurricane strength on 26 December 2016. News sources reported that hurricane strength winds (over 32.6ms^{-1}) were measured for over ten minutes, at a site along the coast near Stavanger (Tatone, 2016).

Schirle et al. (2019) also analyze this pulsed snowfall case, but their study defines the

event from 21 December to 23 December. Similar to the deep/upslope snowfall event on 4 November, the MASC showed that the particles had experienced riming, which may explain the high reflectivity values. They define the event by the persistent westerly winds occurring on those days, which support pulsed mountain waves affecting the precipitation (Schirle et al., 2019). On 23 December, the winds shifted and were southerly for 6 hours. During these hours, the precipitation profile was deep and continuous (or upslope) before returning to westerly winds with an intermittent/pulsed profile. This shift in winds occurred between the first and second low pressure systems.

4.0.3.4 Kiruna Deep Snowfall

The MRR detected the start of a deep snowfall event over Kiruna, Sweden on 5 November 2017 that lasted 20.51 hours. The Doppler derived (Ze-S) LWE accumulation was 5.12mm. Fig. 4.22 shows that the snowfall was continuous and extended to 3km. The winds were primarily northerly at $1\text{-}3\text{ms}^{-1}$, and temperatures gradually warming from -6°C to -1°C (Fig. 4.24). The 2D histogram of reflectivity (left panel in Fig. 4.23) contains a narrow structure of increasing radar reflectivity with decreasing height. At higher levels, the reflectivity ranges from 0 dBz to 10dBz, and near the surface (1km AGL and lower), the values range from 10dBz to 17dBz. The corresponding Doppler velocity in the center panel of Fig. 4.23 indicates that the air and particles are moving toward the radar at approximately 1ms^{-1} . There is also a slight increase in velocity near the surface as well. The spectrum width throughout the column is low and invariant remaining near

0.25ms^{-1} (right panel in Fig. 4.23). There is no apparent spread in particle motions; this suggests that there is little variation in sizes/masses/densities at a given height. The increasing radar reflectivity with decreasing height and the slight increase in Doppler velocity may be consistent with snowflake aggregation and/or riming.

This deep snowfall event was associated with a weak low pressure system over northern Scandinavia (left panel in Fig. 4.25). From the right panel in Fig. 4.25, we can see that compared to the November climatology, there is a weak low pressure anomaly over Northern Scandinavia and weak high pressure anomalies west and east of the region that fit well with the northerly winds, and suggests the Barents Sea was a local moisture source for the precipitation. The left panel in Fig. 4.26 shows that in the vertical structure of temperature there was a weak temperature inversion just below 900mb with little change throughout the 20 hours. The temperatures are also relatively warm in the column below 900mb, temperatures are near -5°C and approaching 0°C , which supports the aggregation of particles because the warmer temperatures allow the particles to more easily stick to each other through (Houze Jr, 2014, Lamb and Verlinde, 2011). The RH profile in the right panel in Fig. 4.26 has some variations near 800mb from 80% to over 100%, but in general, the boundary layer through the free atmosphere is near/at saturation.

4.0.3.5 Kiruna Shallow Snowfall

The shallow snowfall case in Kiruna on 6 February 2018 lasted approximately 40 hours with very little LWE accumulated at the surface- 2.53mm. This snowfall event occurs under very cold temperatures, the event starts near -14°C and decreases to -24°C , and weak northerly winds, $1-3\text{ ms}^{-1}$, and the relative humidity decreases with temperature as well (Fig. 4.27). The semi-continuous profile of precipitation detected by the MRR contains low radar reflectivity ranging from 5dBz to 7dBz (Fig. 4.29). The snowfall profile is shallow with all of the observations below 0.8 km, and the Doppler velocity values are confined to 0.5ms^{-1} (center panel in Fig. 4.29). The observed values for spectrum width shown in the 2D histogram (right panel in Fig. 4.29) are low indicating smooth, gentle snowfall.

The maps of mean sea level pressure, 500mb geopotential height, and their respective anomalies in Fig. 4.30 show that the shallow snowfall event is associated with a persisting high pressure system over the region (left). There is a large high pressure anomaly in the Barents Sea and northern part of Scandinavia, and a secondary region of anomalous high pressure over the North Sea as well (right). In Fig. 4.31, the vertical structure of the atmosphere has a strong temperature inversion, and the RH profile shows that the moisture is contained within the shallow boundary layer. Throughout this long-lived event, there are very little changes in this structure. The persistent high pressure and northerly winds suggest that cold, dry air was advected from the cold, Arctic north.

4.0.3.6 Kiruna Intermittent Snowfall

On 7 December 2017, the MRR detected intermittent snowfall starting at 1607 UTC, and after 76.3 hours led to 12.32mm LWE accumulation. The winds were from the south-east during the event and temperatures increase as the precipitation event progresses (see Fig. 4.32): starting near -20°C , and warming to more than -5°C near the end of the event. This on-and-off precipitation event had periods of high reflectivity, low reflectivity and no precipitation at all (Fig. 4.33). The 2D histogram of radar reflectivity in left panel in Fig. 4.34 illustrates the range is broad along the column ranging from -5dBz to 20dBz , and the range in radar reflectivity values increases approaching the surface. The 2D histogram of Doppler velocity in the center panel of Fig. 4.34 shows that terminal velocity of the particles and the motion of the air went towards the radar at $0.5 - 1.7\text{ms}^{-1}$ with a large increase and broadening near the radar. The increase in Doppler velocities may suggest particles riming and falling more quickly towards the radar. And throughout most of the column, the spectrum width values are low (see the right panel in Fig. 4.34). But it is apparent that near the surface (lower than $.5\text{km}$) there is an increase in spectrum width indicating more turbulent motions. This could indicate a spread in particle sizes as particles with different sizes, masses and densities would fall to the radar at different velocities.

The synoptic scale context shown in Fig. 4.35 of this intermittent snowfall event includes a deep low pressure system off the coast of the Scandinavian peninsula. The pressures reach

as low 970mb and there is a clear trough south-west of the region over central Europe. In the climatological context (right panel in Fig. 4.35, this is a large low pressure anomaly over the region with a high pressure anomaly south of Greenland in the North Atlantic. The vertical profile of temperature (left panel in Fig. 4.36) does not vary dramatically throughout the time of the event; and near the surface, the temperature range in the column coincides with the dendritic growth zone of snowflakes. The relative humidity near the surface does not vary near the surface, but in the free atmosphere there are large oscillations between 60% to 110% RH.

4.0.3.7 Snow Virga

The MRR detects the occurrence of virga, when snowfall sublimates as it falls through the column (Souverijns et al., 2017). A snow virga event was captured by the MRR on 1 December 2017 at 1334 UTC for approximately 3 hours with very little accumulated at the surface. The winds are from the south-west at mostly 3-5 ms^{-1} , with some values exceeding 5 ms^{-1} (windrose in Fig. 4.37). As the surface temperature increases from -8°C to -6.5°C , the relative humidity decreases (Fig. 4.37). The profile in Fig. 4.38 has continuous precipitation aloft with high reflectivity values (over 25 dBz), and rapidly weakening reflectivity values with decreasing height. In the 2D histogram of radar reflectivity in the left panel of Fig. 4.39, the difference in reflectivity aloft and below is strongly apparent. Values reach nearly 25dBZ and are no lower than 10 dBz above 1.5 km AGL, while at 0.5 km AGL the values range from 0 to 10 dBz. In addition to the range of reflectivity values,

the 2D histogram reveals that the majority of the observations are made at higher levels.

The center histogram in Fig. 4.39 of Doppler velocity shows that there is a large spread in velocities towards the radar. Some particles are moving very quickly approaching 3 ms^{-1} while other fall more slowly at $.5 \text{ ms}^{-1}$. The spectrum width values (right panel in Fig. 4.39) are near $.3 \text{ ms}^{-1}$ throughout the column. While there is a large spread in the reflectivity and Doppler velocity, the spectrum width shows that the air in the column is not turbulent.

The mean sea level pressure map in Fig. 4.40 (left) reveals that the event is associated with a low pressure system approaching the site from the North, which is also anomalously low pressure (see right panel in Fig. 4.40), and over the North Atlantic there is anomalously high mean sea level pressure. The vertical profiles of temperature and relative humidity (left and right respectively in Fig. 4.41) both have strong inversions. Within the three hour event, the variations in the thermodynamic profiles are very small. At higher pressure levels, the free atmosphere appears to have high RH, and decreases 700-900mb, and while increasing again at the surface, but does not exceed saturation found above the temperature inversion (below 900 mb).

4.0.4 Results Figures

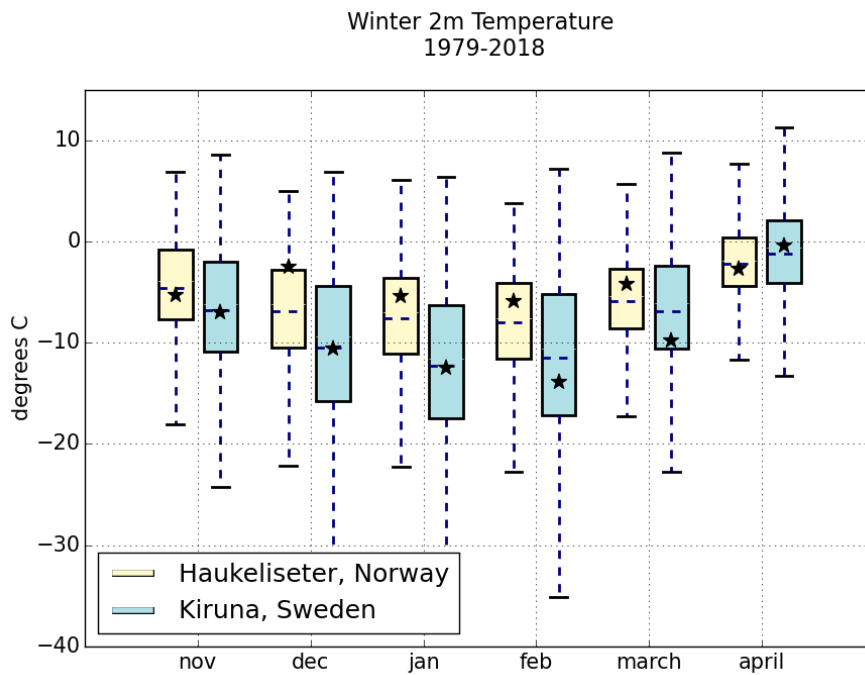


FIGURE 4.1: Box & Whisker plot for mean monthly temperature distributions at sites for winter months (November-April) 1979-2018. The horizontal dashed lines represent the mean temperature of the month for the entire climatological period. The boxes span the interquartile range and the whiskers show the highest and lowest value (excluding outliers). The mean monthly temperature during months of the deployments are superimposed as black stars onto the respective boxes.

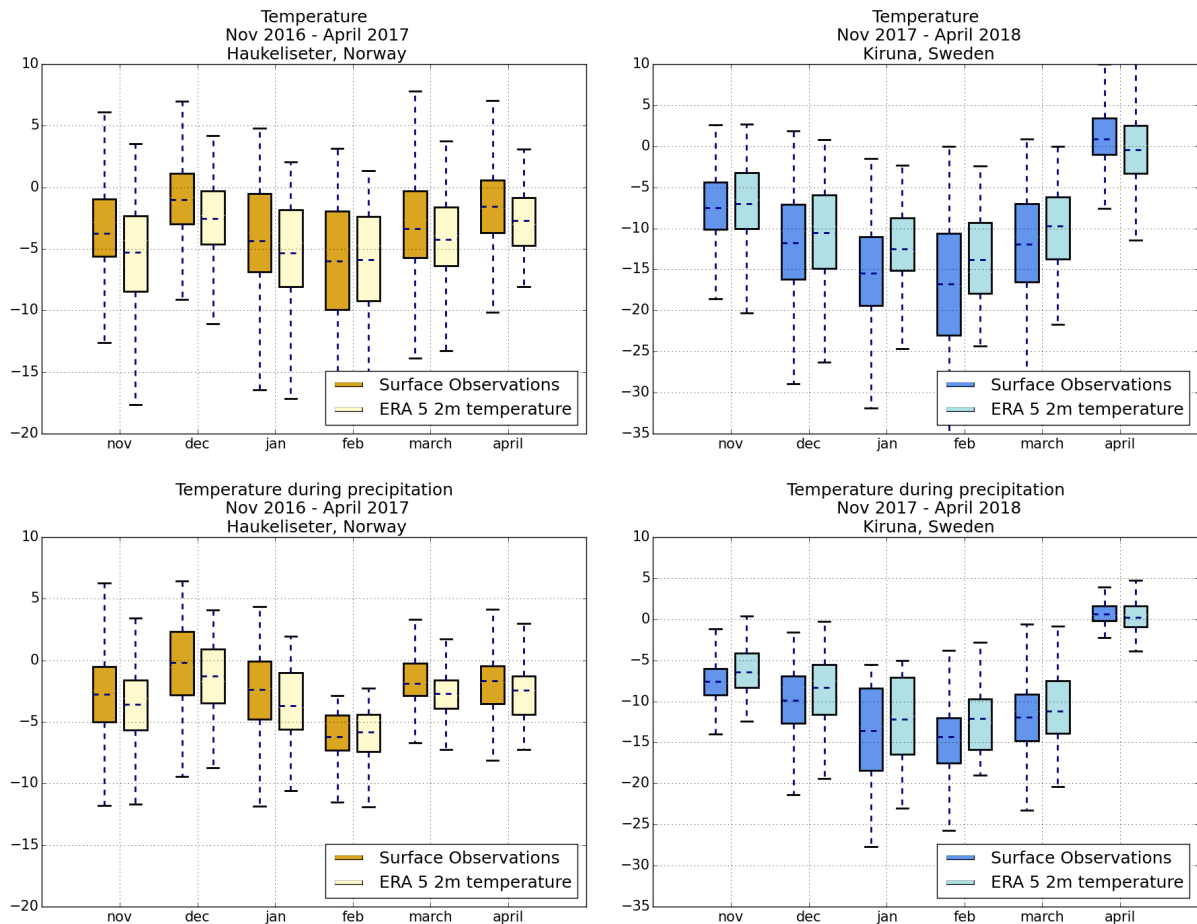


FIGURE 4.2: Box & Whisker plots of monthly distributions from surface temperature observations and ERA5 2m temperature for the months during winter months (November-April) in 2016-2017 in Haukeliseter and 2017-2018 in Kiruna. The left column figures are for distributions in Haukeliseter and the right are for Kiruna, Sweden. The upper figures are for the temperature distribution of the full month; the bottom figures are temperature distributions during precipitation events.

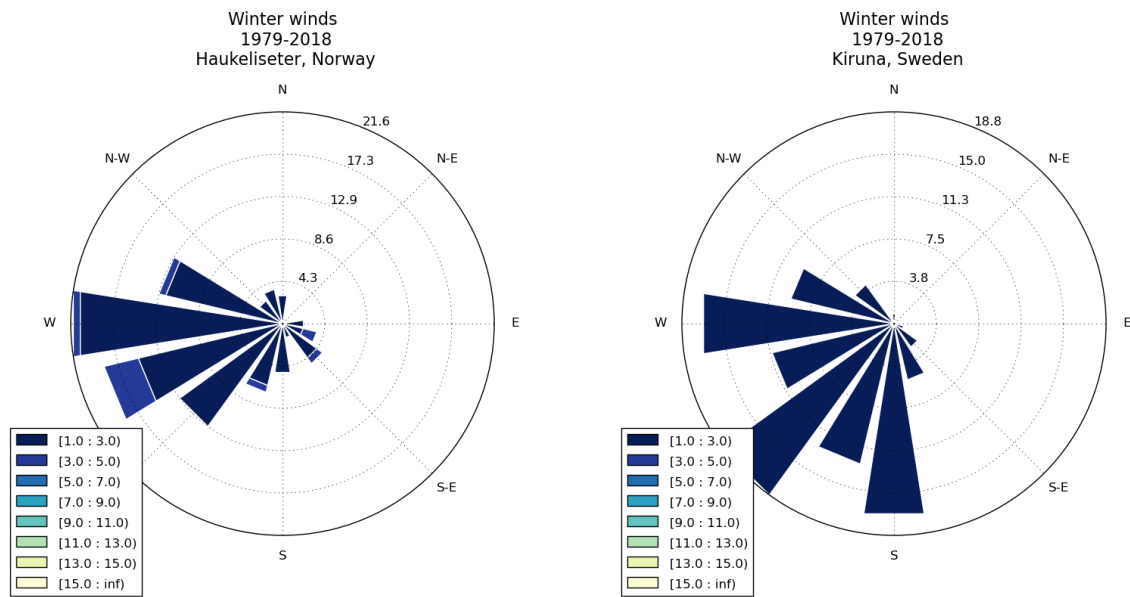


FIGURE 4.3: Windroses of the winter climatology at each site of ERA5 10m winds. The climatological winter period is for November-April from 1979 to 2018. Left: winter winds in Haukelisetser. Right: winter winds in Kiruna. Colors represent wind speed in units of ms^{-1} . The quadrant provides information on the source direction and the size of the rose shows the frequency.

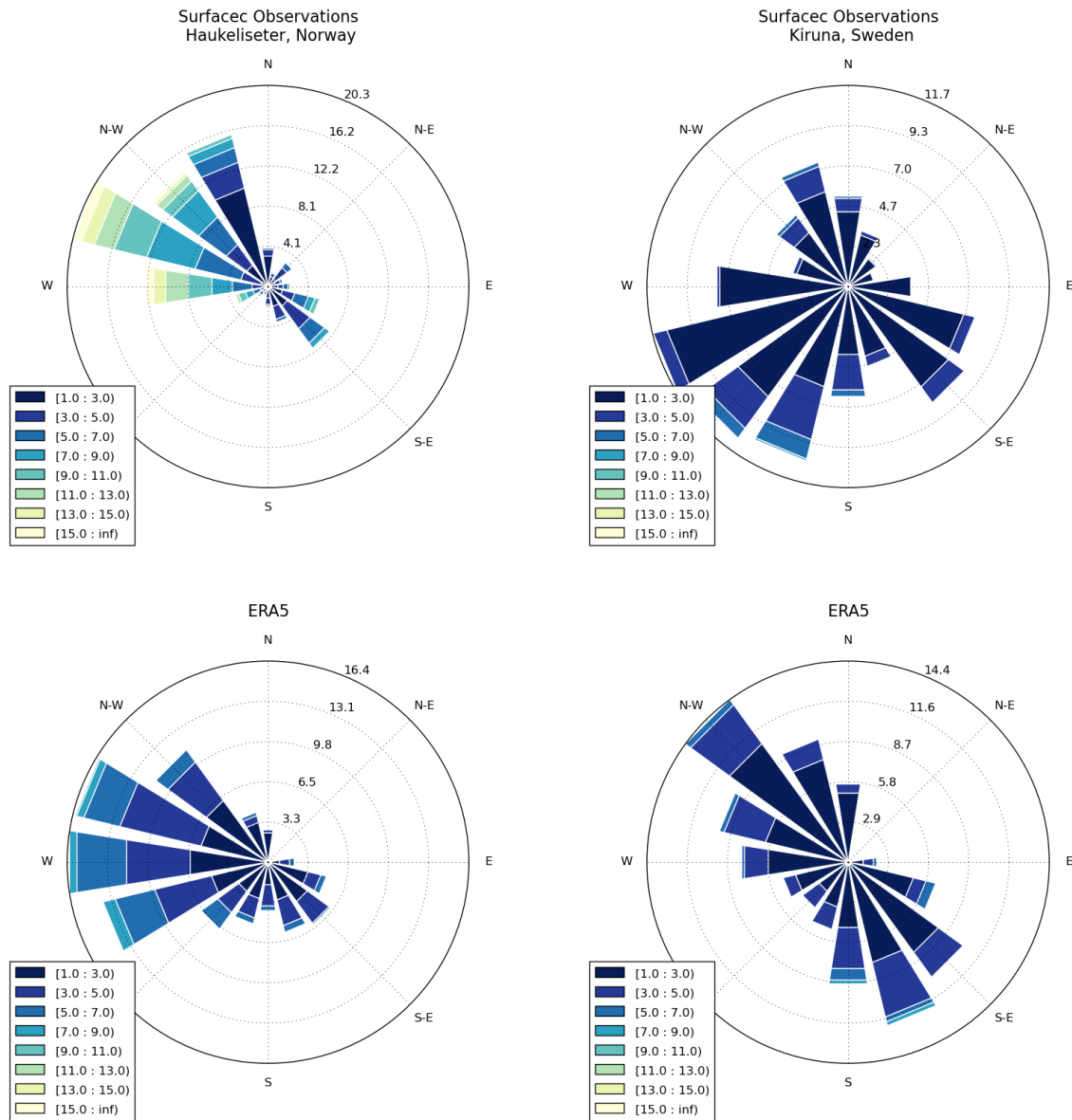


FIGURE 4.4: Windroses of monthly distributions of surface wind observations and ERA5 10m winds during winter months (November-April) in 2016-2017 in Haukeliseter and 2017-2018 in Kiruna. Colors represent wind speed in units of ms^{-1} . The left column figures are for distributions in Haukeliseter and the right are for Kiruna, Sweden. The upper figures are for the winds from surface observations; the bottom figures are the 10m winds from ERA5 reanalyses.

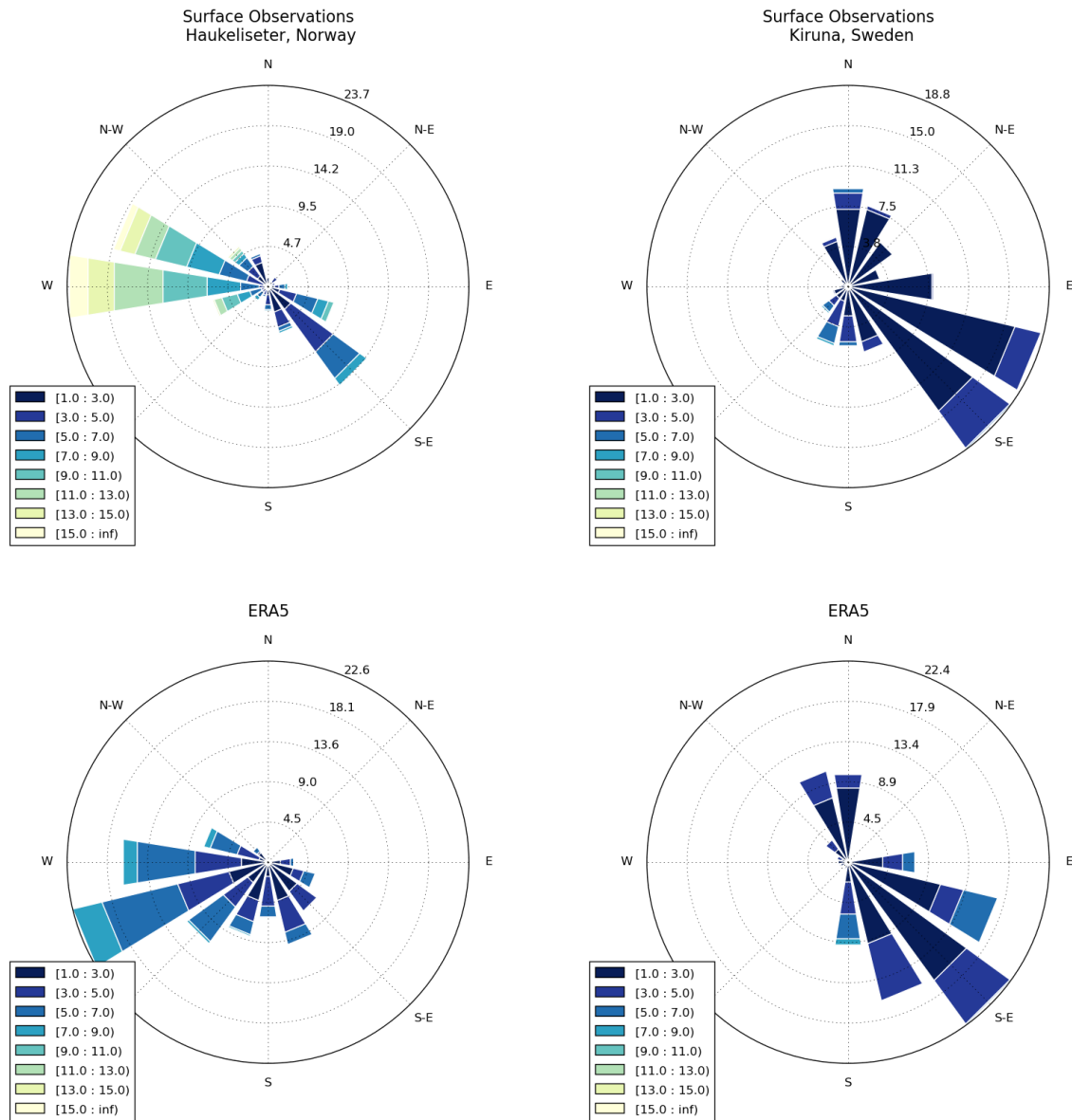


FIGURE 4.5: Windroses during precipitation of monthly distributions of surface wind observations and ERA5 10m winds in the winter months (November - April) in 2016-2017 in Haukeliseter and 2017-2018 in Kiruna. The left column figures are for distributions in Haukeliseter and the right are for Kiruna, Sweden. The upper figures are for the winds from surface observations; the bottom figures are the 10m winds from ERA5 reanalyses.

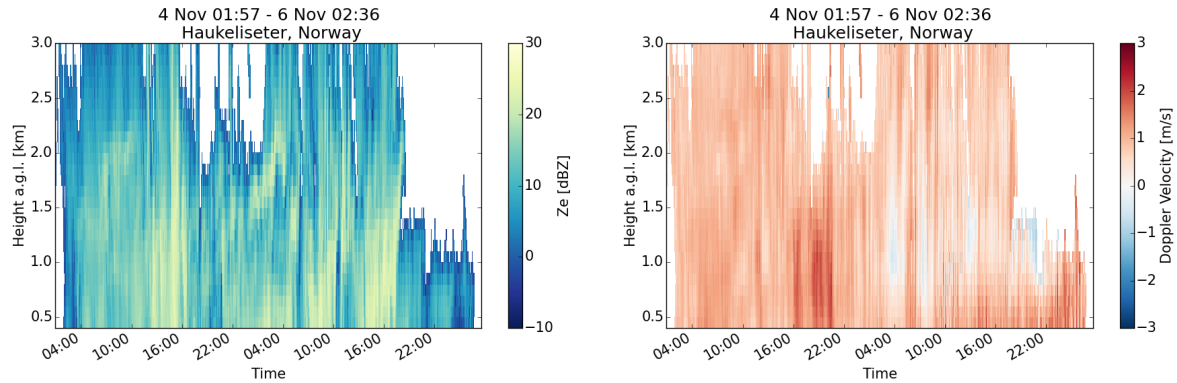


FIGURE 4.6: Radar profiles during deep snowfall event in Haukeliseter, Norway from 4 November 2016 (0157 UTC) - 6 November 2016 (0236 UTC). Left: time x height profile of radar reflectivity (Z_e). Right: time x height profile of Doppler Velocity (V_d).

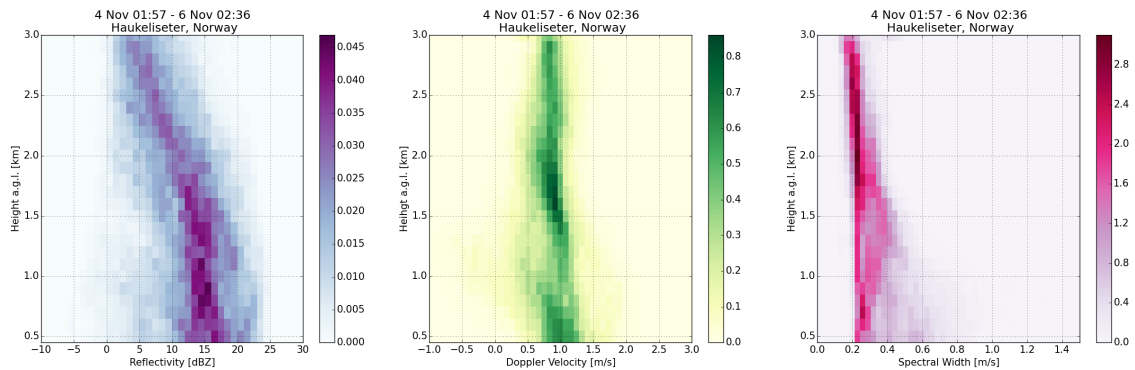


FIGURE 4.7: Left: 2D histogram of Z_e ; Center: 2D histogram of V_d ; Right: 2D histogram of σ . Color-bar & values represent bin count normalized with the total number of observations

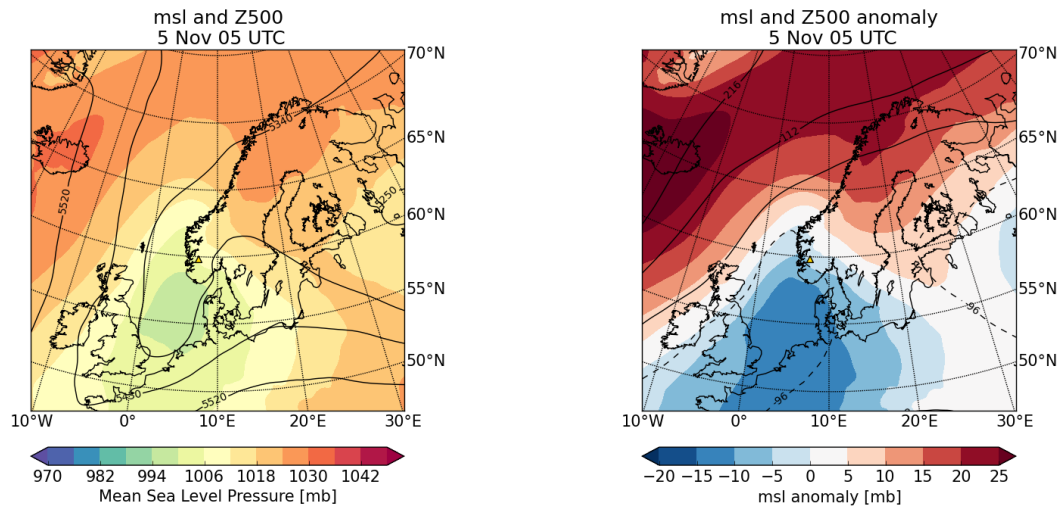


FIGURE 4.8: Synoptic & Climatological context of a given hour during snowfall event: 5 November 2016 0500 UTC. For synoptic context (left): mean sea level pressure (msl) in mb is in the shading and 500mb geopotential height (z500) contours are overlaid. Climatological context (right): msl anomaly in shading and z500 black line contours; negative z500 anomalies are dashed.

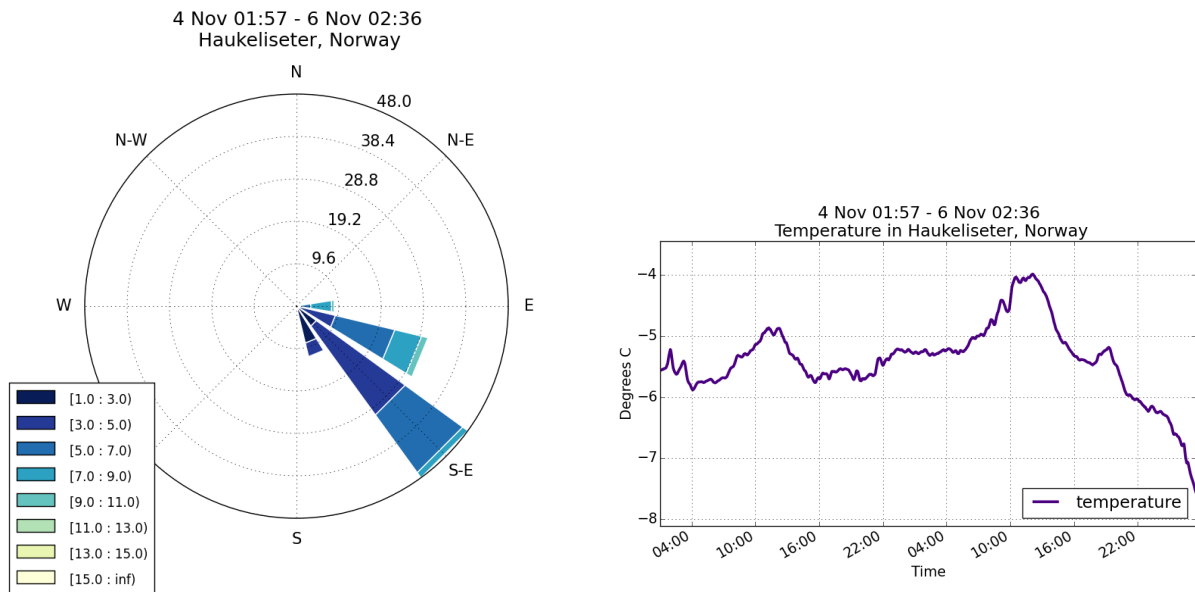


FIGURE 4.9: Meteorological Surface Observations. Left: 10m winds during event. Right: Temperature observations during event smoothed with 15 minute running mean.

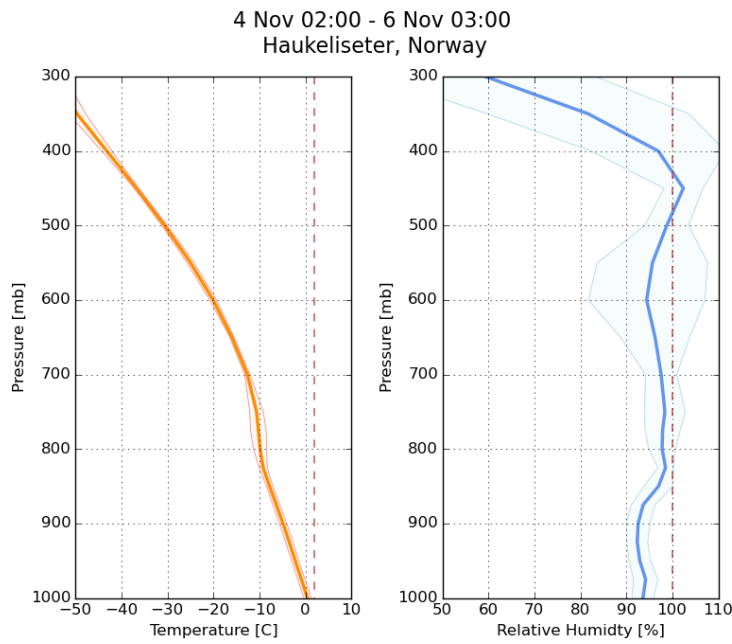


FIGURE 4.10: Average vertical Profiles of temperature and relative humidity from ECMWF ERA5 reanalyses during event. Left: Temperature & dashed line at 2°C indicates temperature threshold between snow and rain; Right: Relative humidity & dashed line is 100% relative humidity with respect to water. Shading represents range between average profile and standard deviation below and above

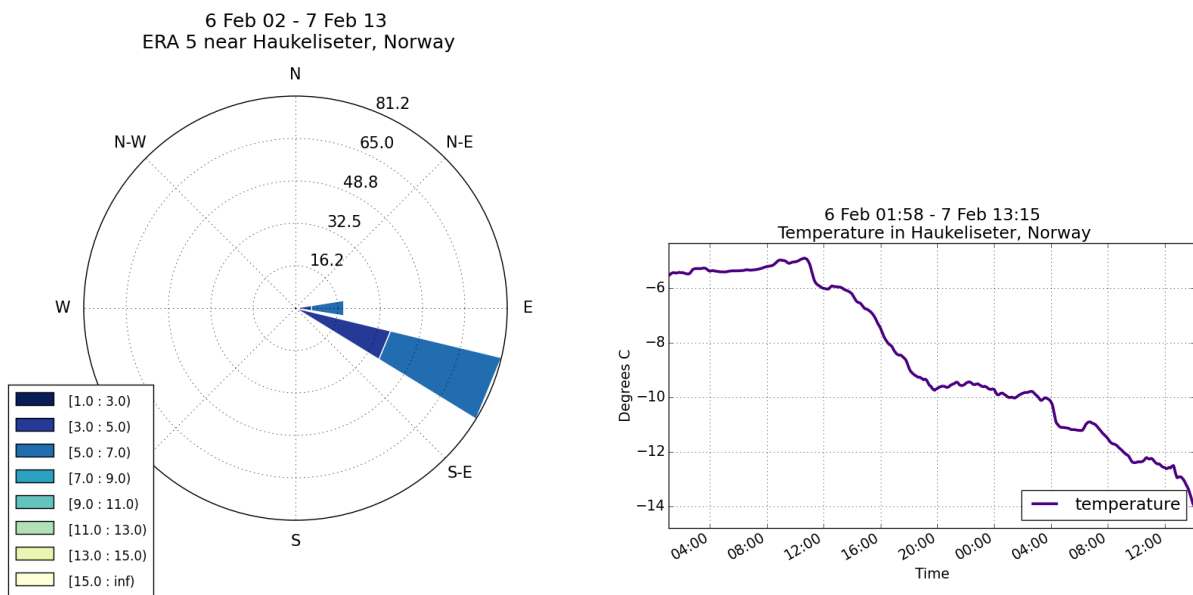


FIGURE 4.11: Left: ERA5 10m winds during event (0200UTC - 1300UTC). Right: Meteorological Surface Temperature observations during event

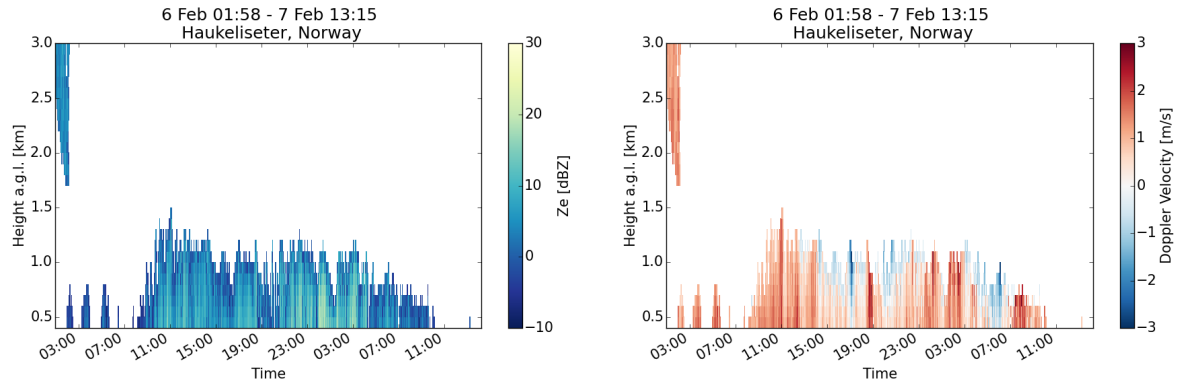


FIGURE 4.12: Radar profiles during shallow snowfall event in Haukelisetser, Norway from 6 February 2017 (0158 UTC) - 7 February 2017 (1315 UTC). Left: time x height profile of radar reflectivity (Z_e). Right: time x height profile of Doppler Velocity (V_d).

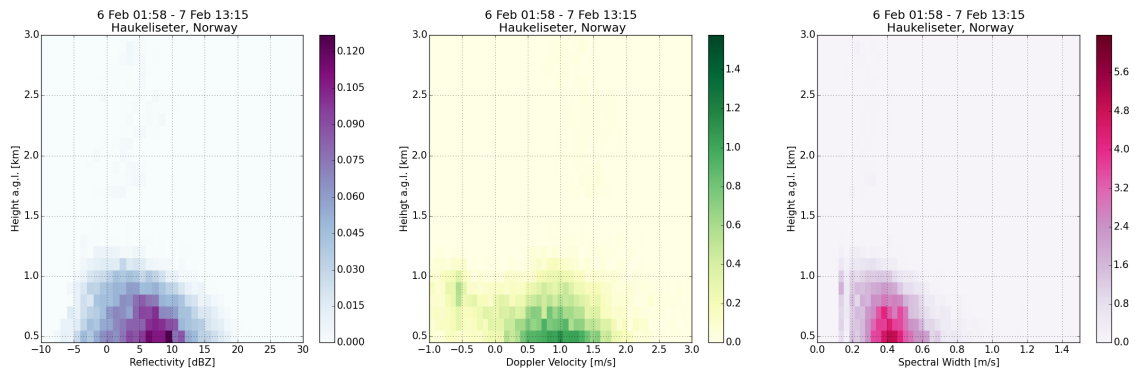


FIGURE 4.13: Left: 2D histogram of Z_e ; Center: 2D histogram of V_d ; Right: 2D histogram of σ . Color-bar & values represent bin count normalized with the total number of observations

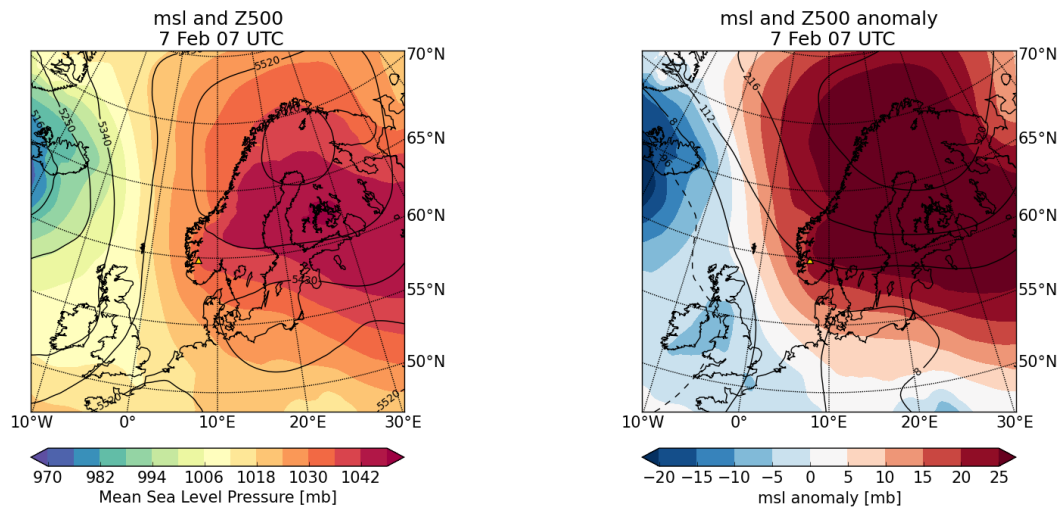


FIGURE 4.14: Synoptic & Climatological context of a given hour during snowfall event: 7 February 2017 0700 UTC. For synoptic context (left): mean sea level pressure (msl) in mb is in the shading and 500mb geopotential height (z500) contours are overlaid. Climatological context (right): msl anomaly in shading and z500 black line contours; negative z500 anomalies are dashed.

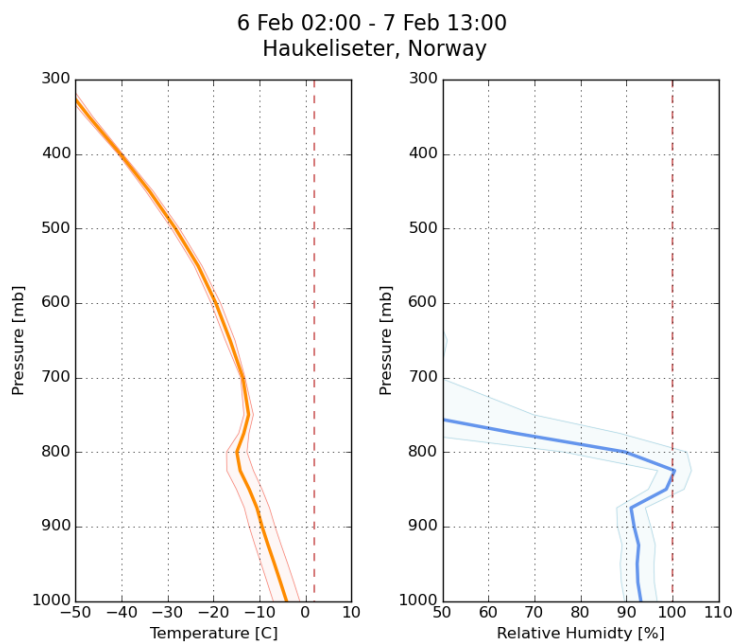


FIGURE 4.15: Average vertical profiles of temperature and relative humidity from ECMWF ERA5 reanalyses during event. Left: Temperature & dashed line at 2°C indicates temperature threshold between snow and rain; Right: Relative humidity & dashed line is 100% relative humidity with respect to water. Shading represents range between average profile and standard deviation below and above

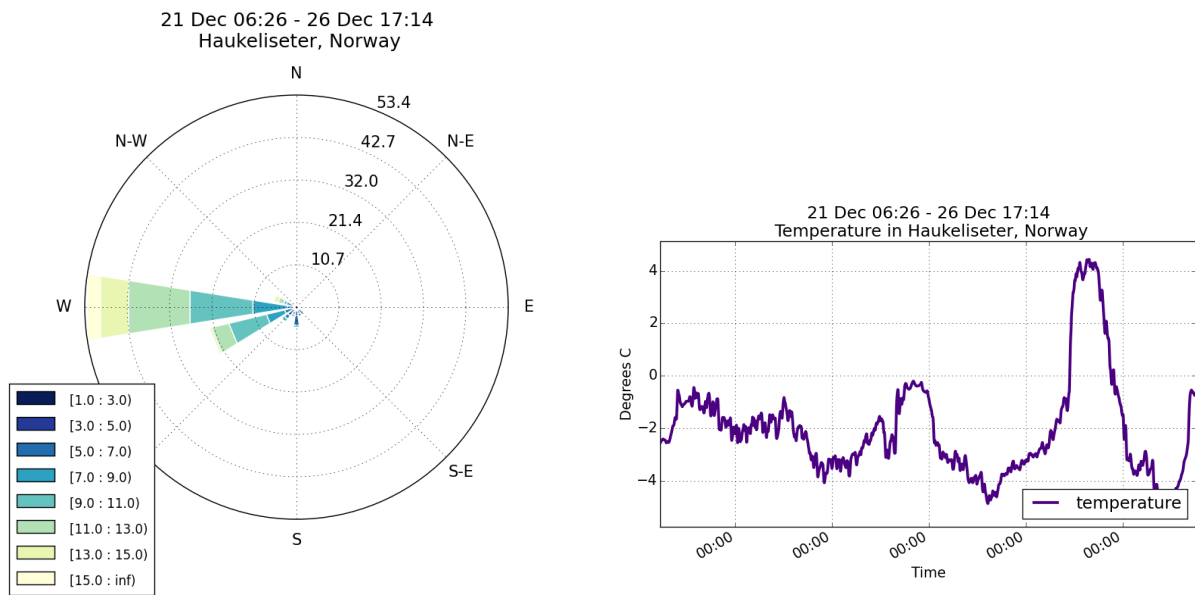


FIGURE 4.16: Meteorological Surface Observations. Left: 10m winds during event. Right: Temperature observations during event smoothed with 15 minute running mean.

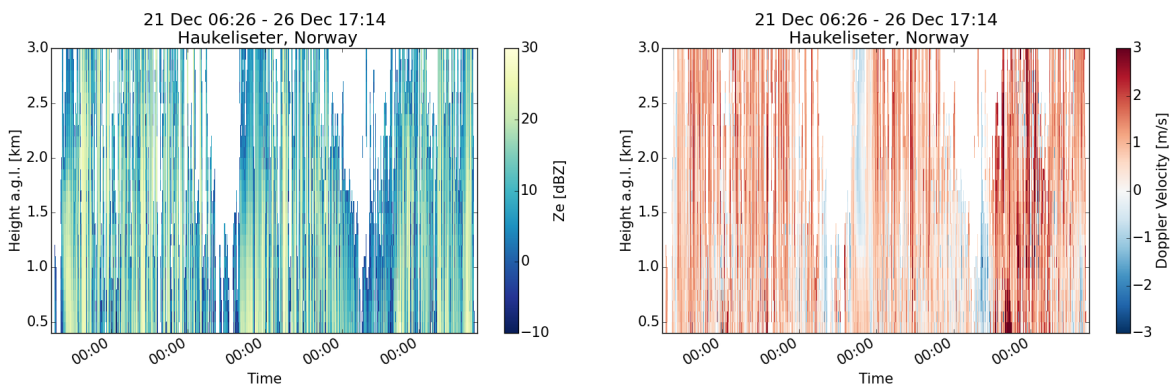


FIGURE 4.17: Radar profiles during shallow snowfall event in Haukelisetser, Norway from 21 December 2016 (0626 UTC) - 26 December 2016 (1714 UTC). Left: time x height profile of radar reflectivity (Ze). Right: time x height profile of Doppler Velocity (Vd).

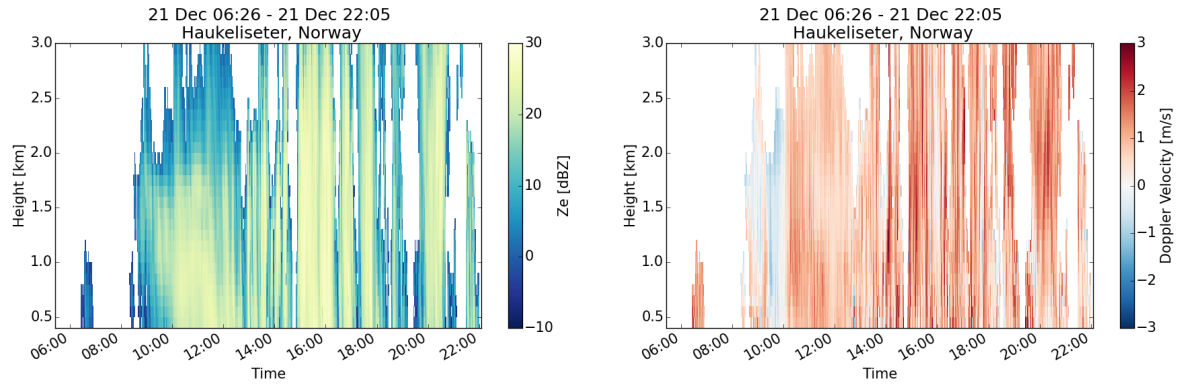


FIGURE 4.18: Zoomed in to the first 16 hours of the Intermittent/Pulsed event in Haukelisetser on 21 December, 2016. Left: profile of radar reflectivity. Right: Profile of Doppler Velocity.

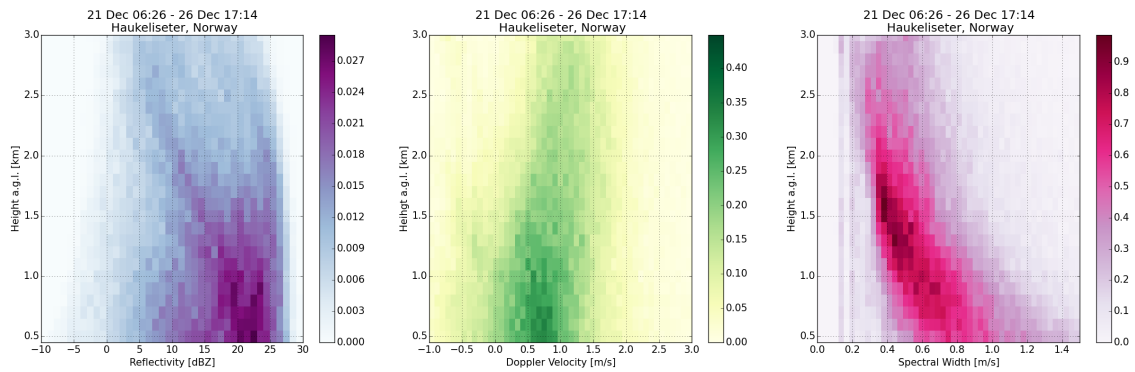


FIGURE 4.19: Left: 2D histogram of Z_e ; Center: 2D histogram of V_d ; Right: 2D histogram of σ . Color-bar & values represent bin count normalized with the total number of observations

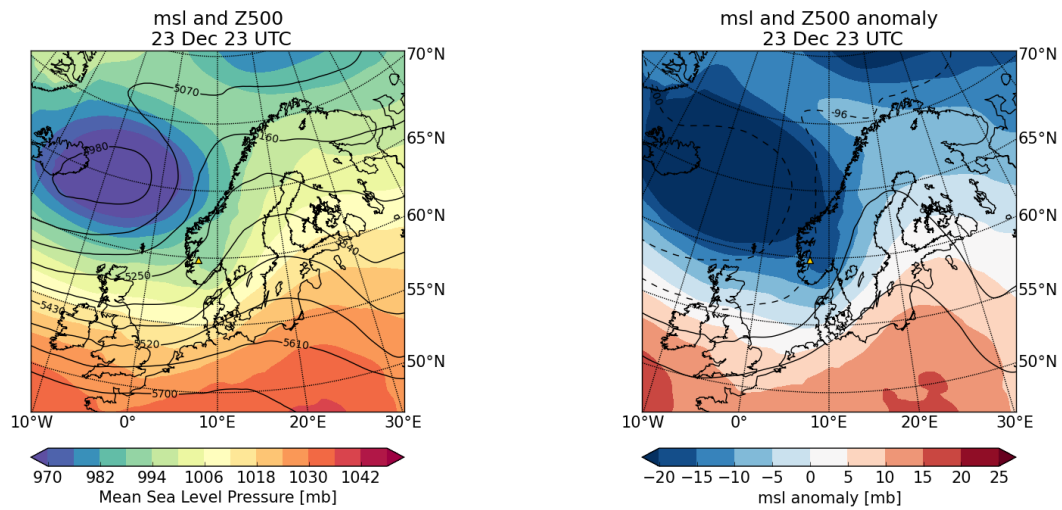


FIGURE 4.20: Synoptic & Climatological context of a given hour during snowfall event: 23 February 2017 2300 UTC. For synoptic context (left): mean sea level pressure (msl) in mb is in the shading and 500mb geopotential height (z500) contours are overlaid. Climatological context (right): msl anomaly in shading and z500 black line contours; negative z500 anomalies are dashed.

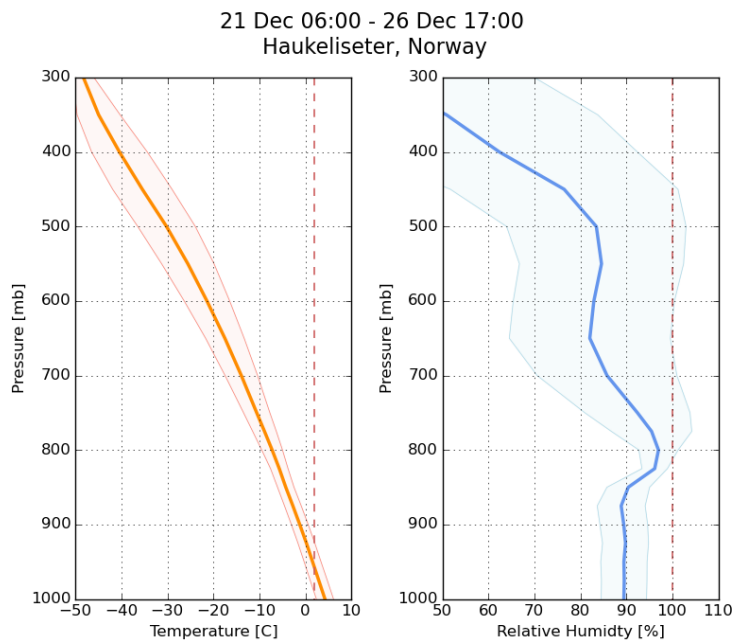


FIGURE 4.21: Average vertical profiles of temperature and relative humidity from ECMWF ERA5 reanalyses during event. Left: Temperature & dashed line at 2°C indicates temperature threshold between snow and rain; Right: Relative humidity & dashed line is 100% relative humidity with respect to water. Shading represents range between average profile and standard deviation below and above

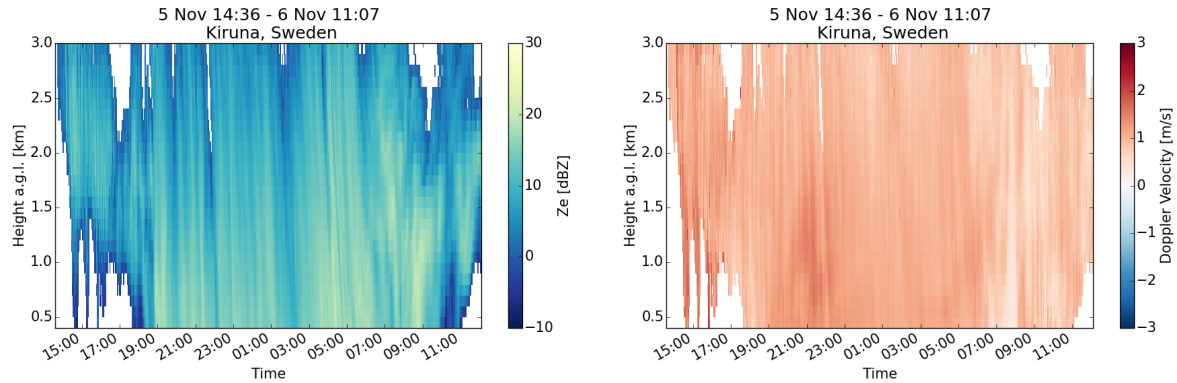


FIGURE 4.22: Radar profiles during shallow snowfall event in Kiruna, Sweden from 5 November 2017 (01436 UTC) - 5 November 2017 (11:07 UTC). Left: time x height profile of radar reflectivity (Z_e). Right: time x height profile of Doppler Velocity (V_d).

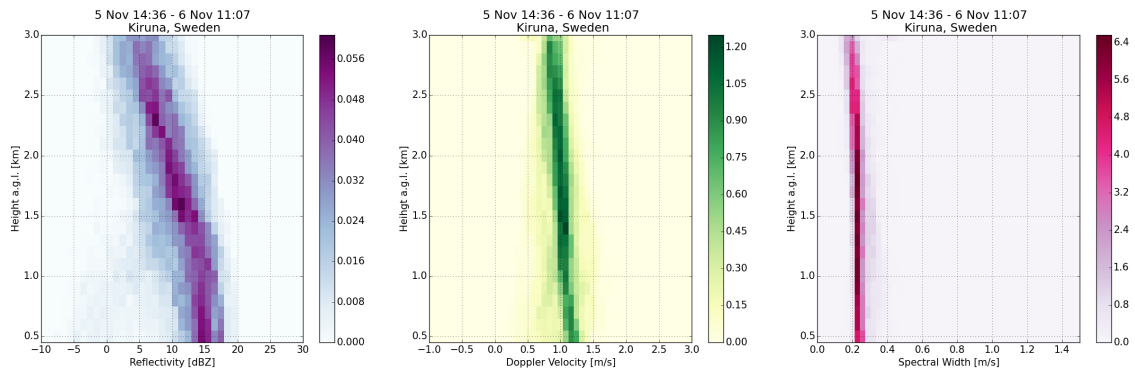


FIGURE 4.23: Left: 2D histogram of Z_e ; Center: 2D histogram of V_d ; Right: 2D histogram of σ . Color-bar & values represent bin count normalized with the total number of observations

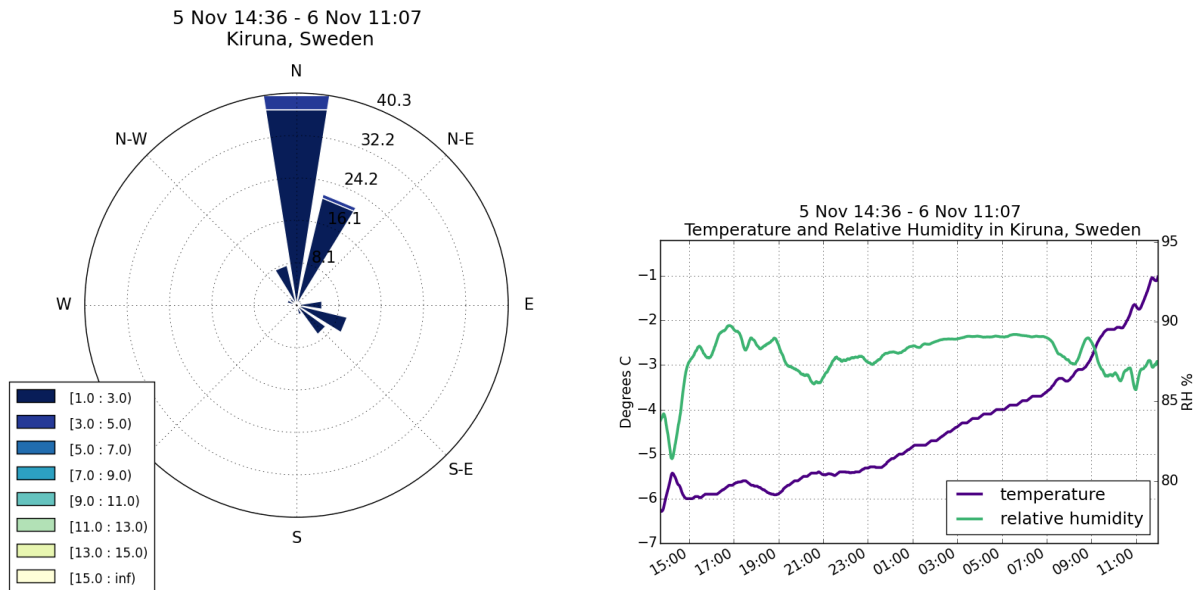


FIGURE 4.24: Meteorological Surface Observations. Left: 10m winds during event. Right: Temperature and relative humidity observations during event smoothed with 15 minute running mean.

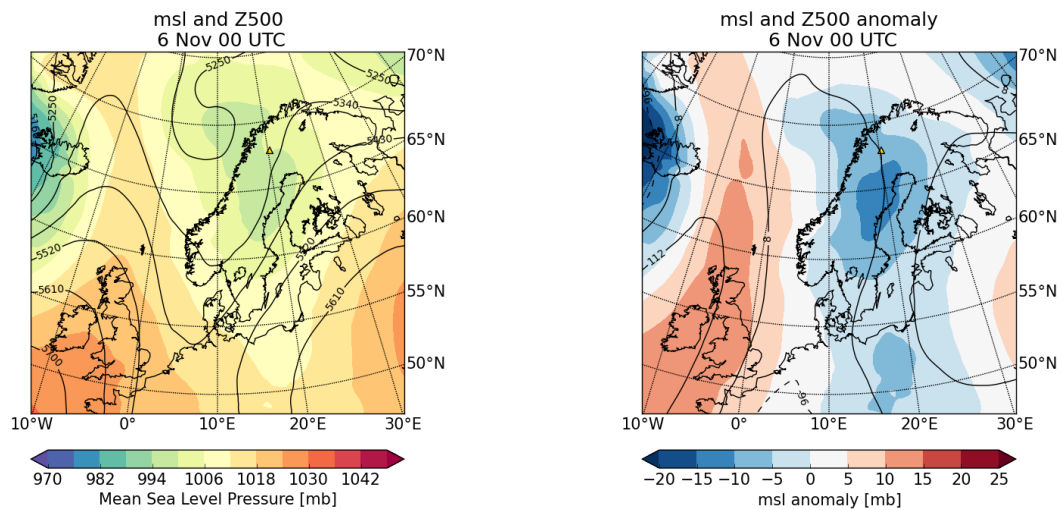


FIGURE 4.25: Synoptic & Climatological context of a given hour during snowfall event: 6 November 2017 0000 UTC. For synoptic context (left): mean sea level pressure (msl) in mb is in the shading and 500mb geopotential height (z500) contours are overlaid. Climatological context (right): msl anomaly in shading and z500 black line contours; negative z500 anomalies are dashed.

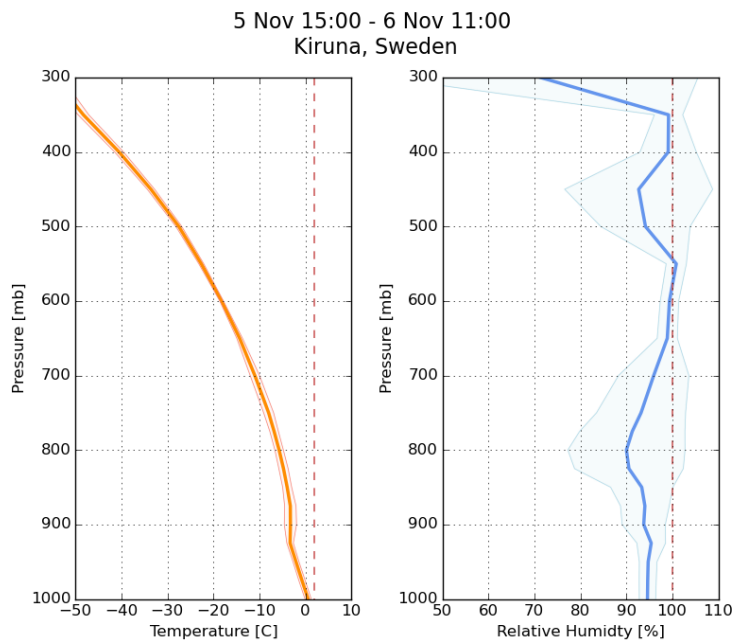


FIGURE 4.26: Average vertical profiles of temperature and relative humidity from ECMWF ERA5 reanalyses during event. Left: Temperature & dashed line at 2°C indicates temperature threshold between snow and rain; Right: Relative humidity & dashed line is 100% relative humidity with respect to water. Shading represents range between average profile and standard deviation below and above

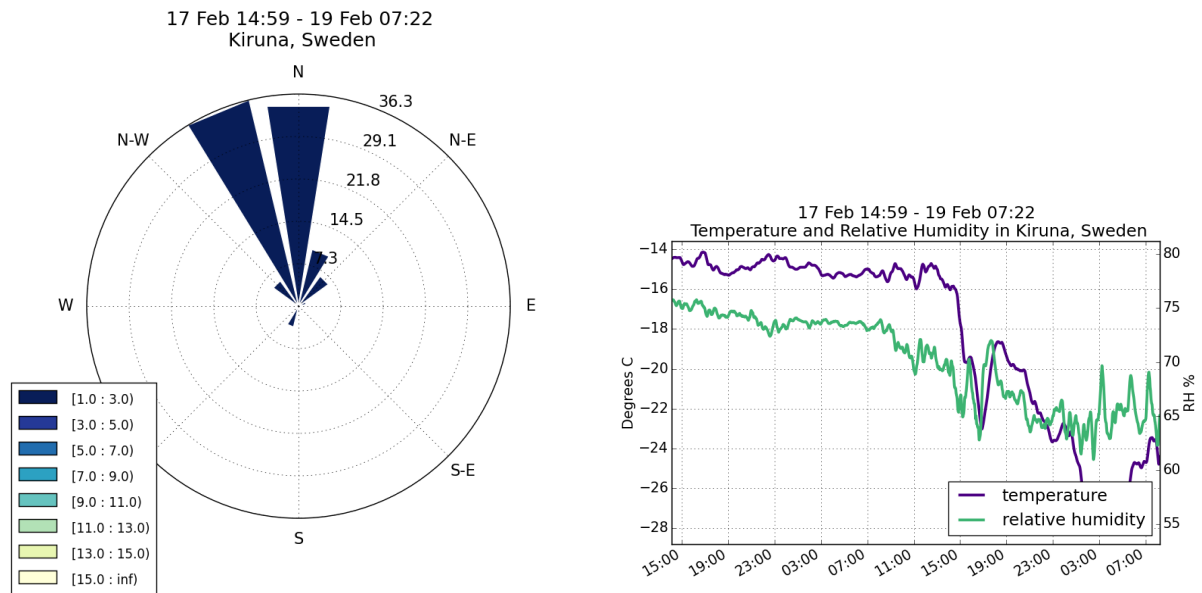


FIGURE 4.27: Meteorological Surface Observations. Left: 10m winds during event. Right: Temperature and relative humidity observations during event smoothed with 15 minute running mean.

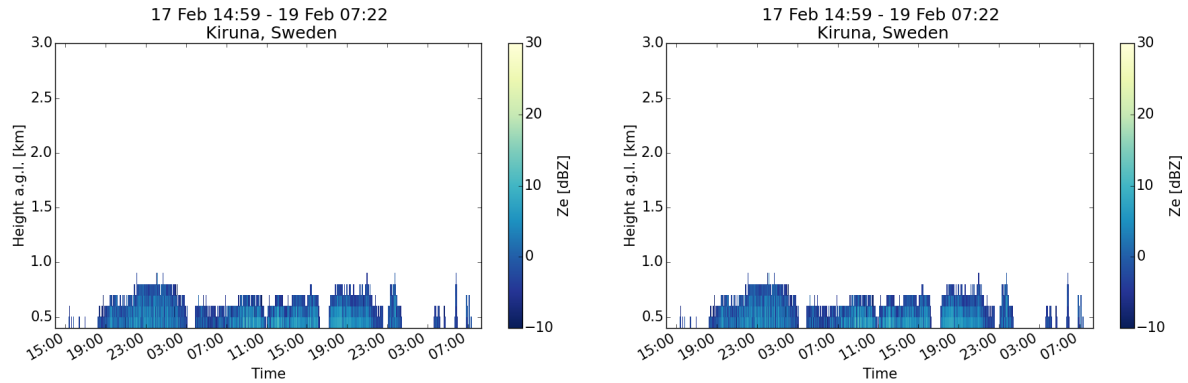


FIGURE 4.28: Radar profiles during shallow snowfall event in Kiruna, Sweden from 17 February 2018 (01459 UTC) - 19 February 2018 (0722 UTC). Left: time x height profile of radar reflectivity (Z_e). Right: time x height profile of Doppler Velocity (V_d).

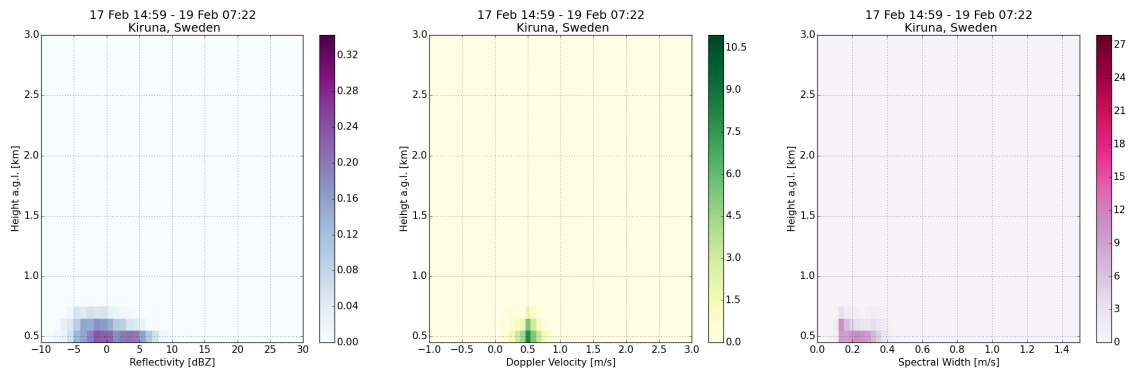


FIGURE 4.29: Left: 2D histogram of Z_e ; Center: 2D histogram of V_d ; Right: 2D histogram of σ . Color-bar & values represent bin count normalized with the total number of observations

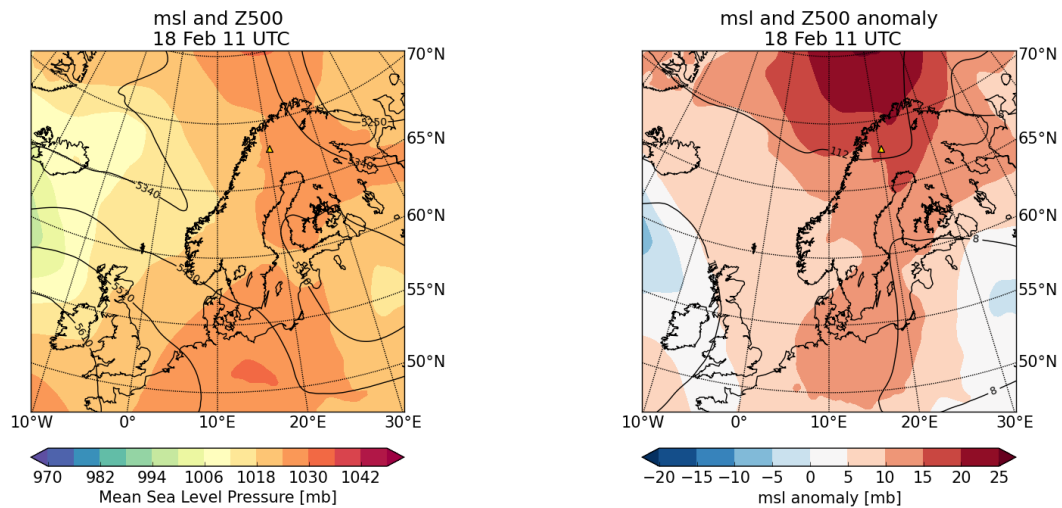


FIGURE 4.30: Synoptic & Climatological context of a given hour during snowfall event: 18 February 2018 1100 UTC. For synoptic context (left): mean sea level pressure (msl) in mb is in the shading and 500mb geopotential height (z500) contours are overlaid. Climatological context (right): msl anomaly in shading and z500 black line contours; negative z500 anomalies are dashed.

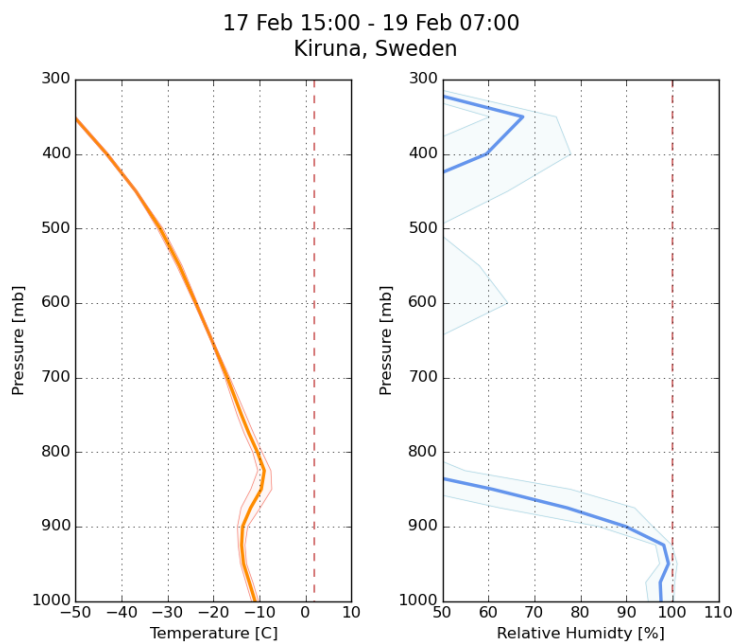


FIGURE 4.31: Average vertical profiles of temperature and relative humidity from ECMWF ERA5 reanalyses during event. Left: Temperature & dashed line at 2°C indicates temperature threshold between snow and rain; Right: Relative humidity & dashed line is 100% relative humidity with respect to water. Shading represents range between average profile and standard deviation below and above

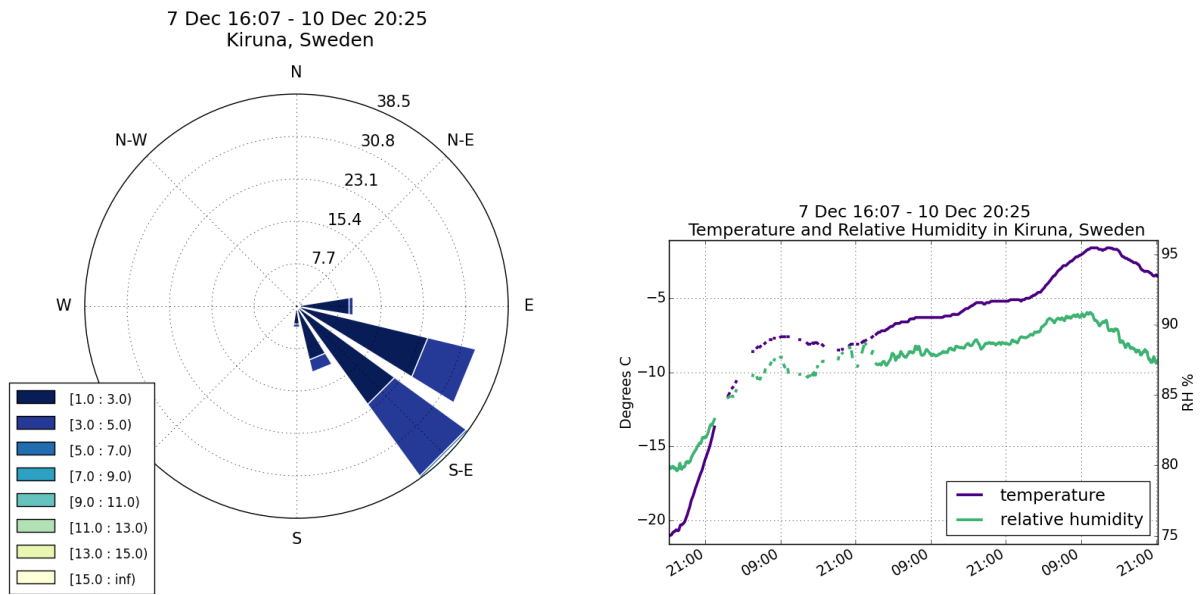


FIGURE 4.32: Meteorological Surface Observations. Left: 10m winds during event. Right: Temperature and relative humidity observations during event smoothed with 15 minute running mean.

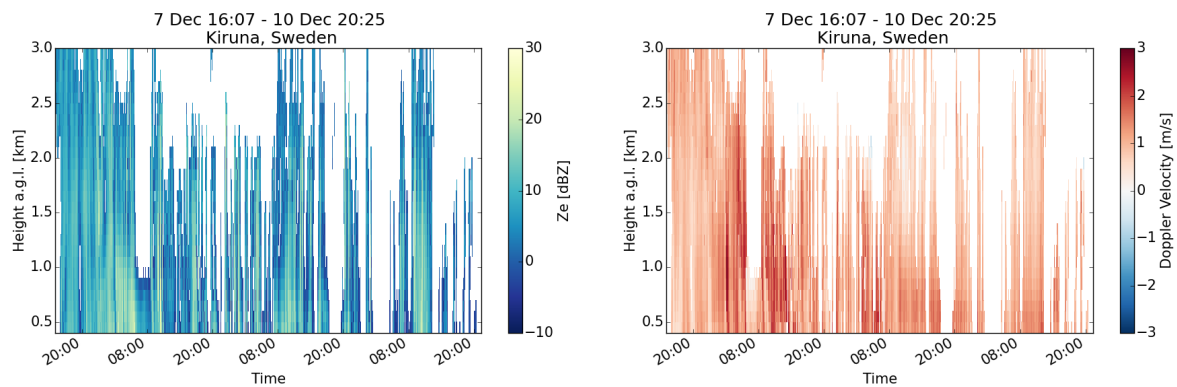


FIGURE 4.33: Radar profiles during shallow snowfall event in Haukeliseter, Norway from 21 December 2016 (0626 UTC) - 26 December 2016 (1714 UTC). Left: time x height profile of radar reflectivity. Right: time x height profile of Doppler Velocity (V_d).

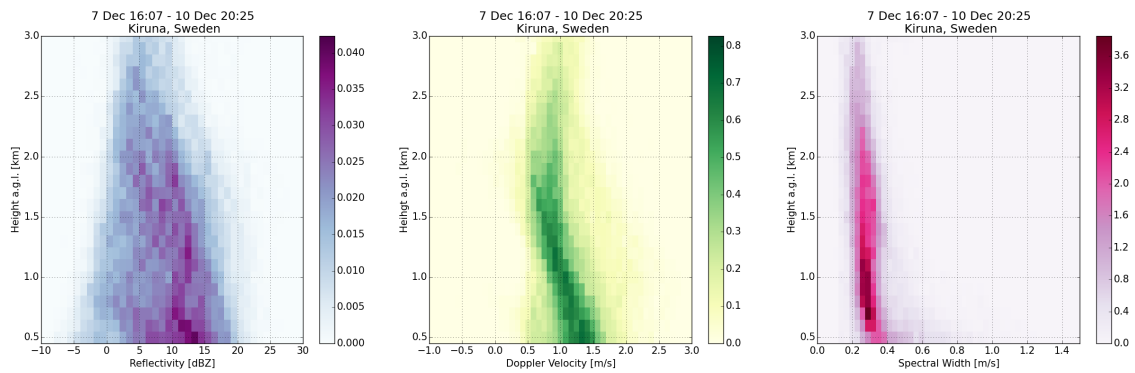


FIGURE 4.34: Left: 2D histogram of Z_e ; Center: 2D histogram of V_d ; Right: 2D histogram of σ . Color-bar & values represent bin count normalized with the total number of observations

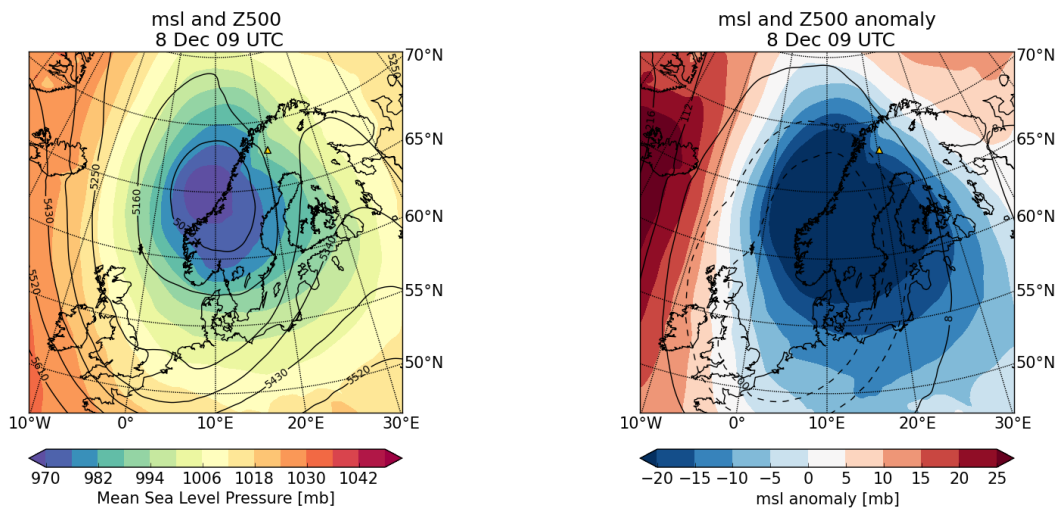


FIGURE 4.35: Synoptic & Climatological context of a given hour during snowfall event: 8 December 2017 0900 UTC. For synoptic context (left): mean sea level pressure (msl) in mb is in the shading and 500mb geopotential height (z500) contours are overlaid. Climatological context (right): msl anomaly in shading and z500 black line contours; negative z500 anomalies are dashed.

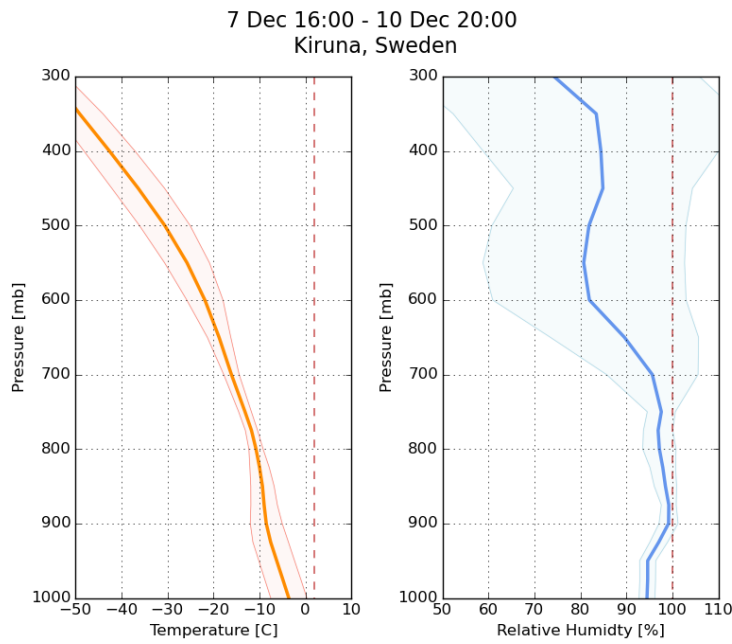


FIGURE 4.36: Average vertical profiles of temperature and relative humidity from ECMWF ERA5 reanalyses during event. Left: Temperature & dashed line at 2°C indicates temperature threshold between snow and rain; Right: Relative humidity & dashed line is 100% relative humidity with respect to water. Shading represents range between average profile and standard deviation below and above

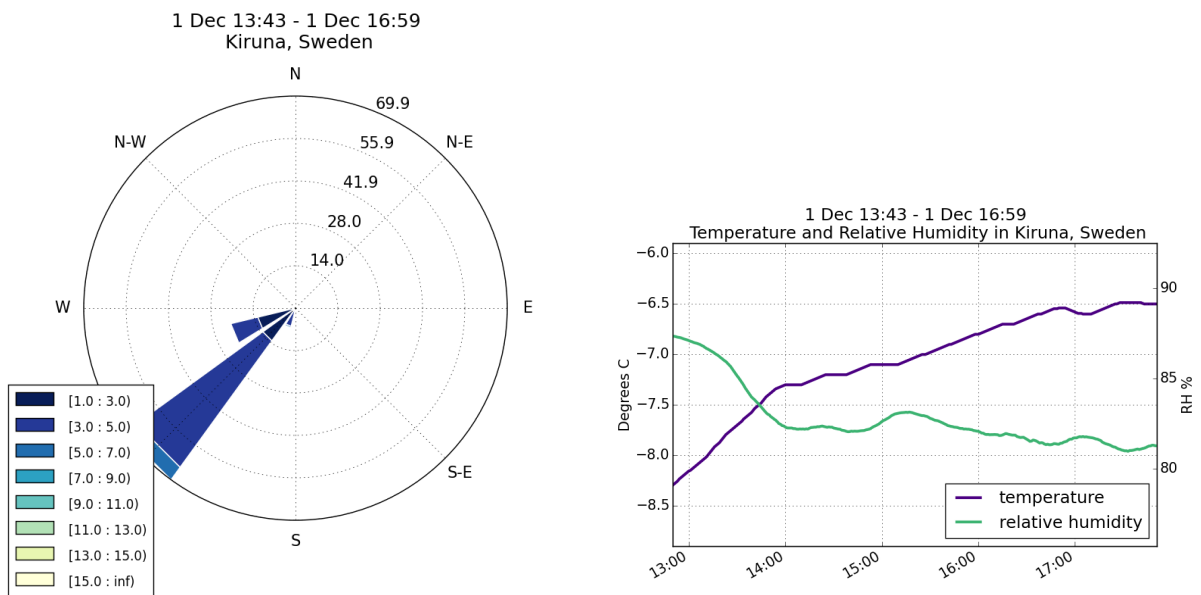


FIGURE 4.37: Meteorological Surface Observations. Left: 10m winds during event. Right: Temperature and relative humidity observations during event

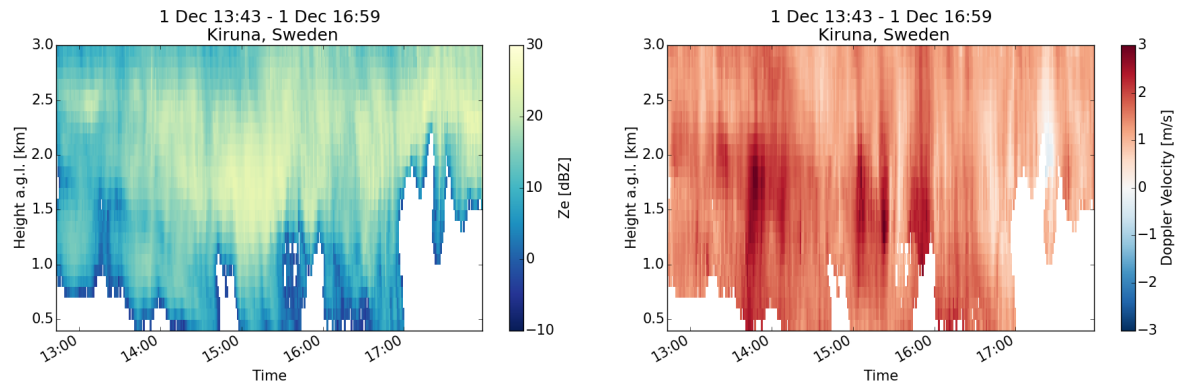


FIGURE 4.38: Radar profiles during shallow snowfall event in Haukelisetter, Norway from 1 December 2017 (1343 UTC) - 1 December 2017 (1659 UTC). Left: time x height profile of radar reflectivity (Z_e). Right: time x height profile of Doppler Velocity (V_d).

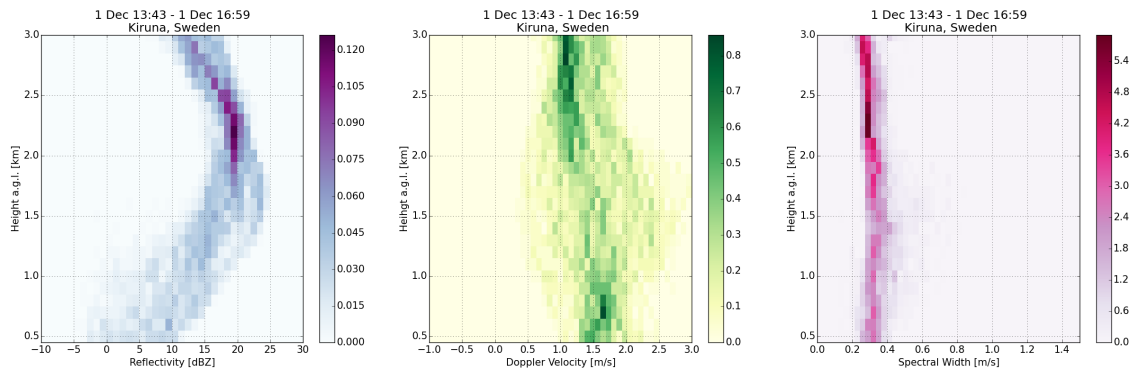


FIGURE 4.39: Left: 2D histogram of Z_e ; Center: 2D histogram of V_d ; Right: 2D histogram of σ . Color-bar & values represent bin count normalized with the total number of observations

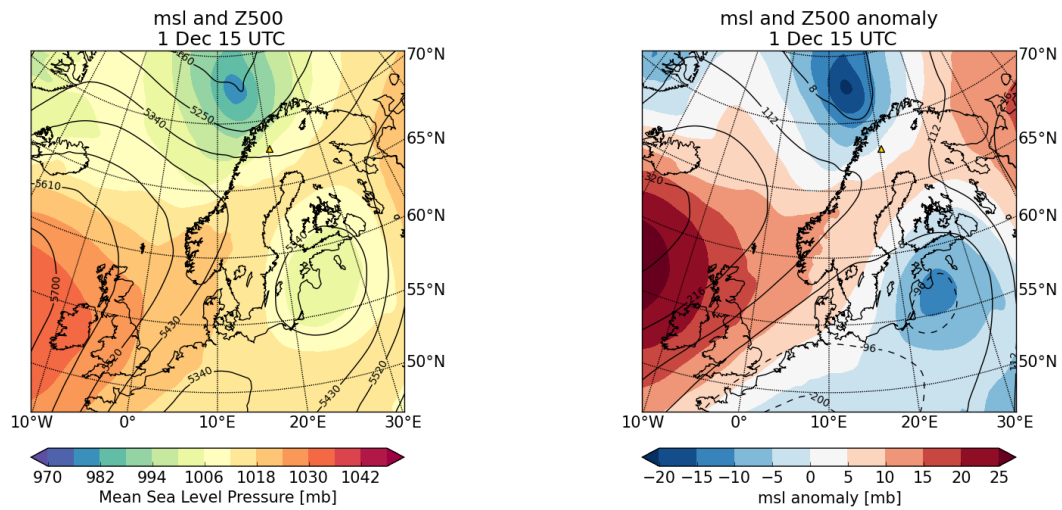


FIGURE 4.40: Synoptic & Climatological context of a given hour during snowfall event: 1 December 2017 1500 UTC. For synoptic context (left): mean sea level pressure (msl) in mb is in the shading and 500mb geopotential height (z500) contours are overlaid. Climatological context (right): msl anomaly in shading and z500 black line contours; negative z500 anomalies are dashed.

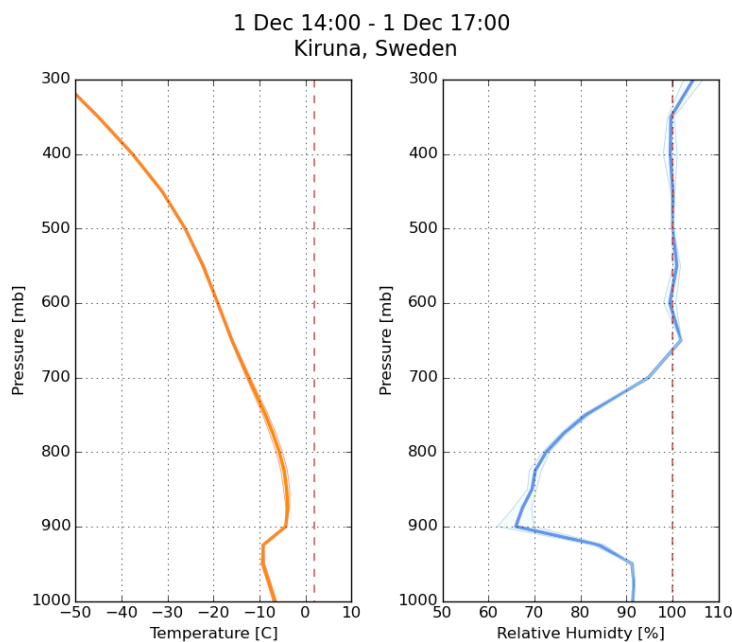


FIGURE 4.41: Average vertical profiles of temperature and relative humidity from ECMWF ERA5 reanalyses during event. Left: Temperature & dashed line at 2°C indicates temperature threshold between snow and rain; Right: Relative humidity & dashed line is 100% relative humidity with respect to water. Shading represents range between average profile and standard deviation below and above

Chapter 5

Discussion and Synthesis

Haukeliseter, Norway and Kiruna, Sweden have unique wind-modes during precipitation events that are different from their respective climatological November-April winds. The winter winds in Haukeliseter are primarily westerly and north-westerly, and during precipitation there are two main wind modes: westerly and south-easterly. The westerly winds are the most affected by the extreme topography, but the south-easterly winds also carry air masses up a slope. In Kiruna, the south-westerly and southerly winds are the most frequent during the winter, but winter precipitation is characterized by northerly and south-easterly winds, with a small percentage of winds from the south-west. In Kiruna, precipitation coincides most frequently with south-easterly and northerly winds where the topography is less complex. On the other-hand, the full season surface winds are dominated by south and south-westerly winds and that direction coincides with the largest mountains in Sweden, which physically may explains why the winds are poorly

represented in the ERA5 during the season. The ERA5 winds match the observations best during precipitation events in Kiruna, but poorly in Haukeliseter during precipitation events (the westerly winds are lower than measured at the surface and the fraction of south-easterly winds is too small). However, the winter climatology (1979-2018) represents that the winter winds are primarily south-westerly. In Haukeliseter, westerly winds dominate throughout precipitating and non-precipitating times, but south-easterly winds also occur during precipitation events. Devasthale and Norin (2014) also found results from the Swedish weather radar network that westerly and south-westerly winds are the most frequent across Sweden.

The wind-modes that are described above correspond to the distinct snowfall regimes in Haukeliseter, but not necessarily in Kiruna. In Haukeliseter, the westerly winds are associated with the intermittent/pulsed snowfall, and the south-easterly winds occur during shallow and deep snowfall events. This is consistent with work done by Schirle et al. (2019) in Haukeliseter where they find high-impact, pulsed snowfall events associated with the westerly winds that contrast with lower-impact, continuous snowfall events from the south-east. In Kiruna, the specific case events/regimes do not appear to necessarily correspond to a specific wind direction.

Across the Scandinavian peninsula, the two sites exhibit snowfall regimes with shared characteristics, albeit with some variations. Table 5.1 summarizes the regimes and the corresponding characteristics. In general, the cases differ because of the differences in the local environment; the synoptic scale context appears to be connected to the similarities

| Regimes & Characteristics | | | |
|---------------------------|-------------------------|-------------------|--|
| Regime | Haukeliseter, Norway | Kiruna, Sweden | Characteristics |
| Deep | ✓ | ✓ | Weak low pressure; Substantial LWE accumulation |
| Shallow | ✓ | ✓ | Persistent high pressure; Low LWE accumulation |
| Intermittent | ✓ | ✓ | Deep low pressure along coast; High LWE accumulation |
| Pulsed | ✓ | | Intermittent snowfall enhanced by local topography |
| Snow Virga | | ✓ | Low pressure from the North; Cold, dry air advection; Low LWE accumulation |

TABLE 5.1: Summary table of snowfall regimes/representative cases at the two Scandinavian sites

in the cases. The deep snowfall events in both Haukeliseter and Kiruna have a defined, narrow structure of increasing reflectivity towards the surface in the 2D histogram of radar reflectivity. Combined with the relatively warm surface temperatures during both of the deep snowfall events, the similar structure in the 2D histograms suggests that the same physical processes (riming and/or aggregation) may also be at play in forming snowflakes. Additionally, the deep snowfall events at each site are associated with a weak low pressure system and advection of moisture. The vertical structure of the atmosphere is characterized by the moistening of the boundary layer through the free atmosphere for the deep snowfall at both sites. The shallow snowfall events at both Haukeliseter and Kiruna exhibit similarities as well, specifically low LWE accumulation under a persistent high pressure. The atmosphere is stable with a strong temperature inversion and moisture is confined to the boundary layer. The shallow snowfall cases differ at each site in that the Doppler velocity and spectral width indicate turbulence in the shallow

precipitation column at Haukeliseter, which could be due to the local complex orography at this site. The intermittent snowfall regimes are also similar at the two sites, but differ in that the turbulence in Haukeliseter enhances the intermittent snowfall and makes it amplified resulting in a pulsed nature of the snowfall. At both Haukeliseter and Kiruna, intermittent snowfall leads to substantial LWE accumulations at the surface. The large-scale atmospheric environment includes a deep low pressure system off the coast of the Scandinavian peninsula. The multiple cyclones in Haukeliseter intermittent/pulsed case could potentially be part of an atmospheric river event; AR's have been associated with multiple cyclones along the coast of Scandinavia in December 2006 (Sodemann and Stohl, 2013). In Kiruna, snow virga is recognized as snowfall regime common to this site, but not to Haukeliseter. The specific case described in the results is short-lived with only 3 hours of precipitation, but it is an extreme example of high radar reflectivities aloft with essentially no precipitation reaching the surface. Snow virga also occurs over the Princess Elizabeth Station in Antarctica, and Souverijns et al. (2017) describe that the near surface sublimation can lead to an overestimation of snowfall rate. Snowfall in Haukeliseter has higher LWE accumulation than in Kiruna between all the cases.

In general, the similarities across the snowfall events at the distinct sites can be connected to the synoptic scale context of the event. And unique characteristics seem to be connected to local topography in Haukeliseter and the presence of drier air in Kiruna. In addition, it is interesting that the conditions also support similar physical mechanisms/processes for the development of snowfall on the microphysical scale. For example,

we speculate that the particles forming in the deep snowfall events experience riming and/or aggregation.

Chapter 6

Conclusions

6.1 Conclusions and Future Directions

By characterizing temperature and wind conditions, and by analyzing observations of snowfall events at two distinct sites in Scandinavia, this research improves our understanding of the role of local environment and large-scale circulation in the development of precipitation in the high-latitudes.

This work determines that there are distinct and recognizable snowfall regimes in southern Norway and Northern Sweden. Despite the large distance between the sites and variations in their topography and surface conditions, it stands out that the snowfall regimes at the distinct sites have similarities. Radar observations reveal precipitation characteristics such as the depth of the precipitation column and how the radar reflectivity values

change with height. Another key finding was that the local environment does impact the snowfall: specifically, the mountains lead to turbulence during snowfall events enhancing the intermittent snowfall in Haukeliseter; and cold, dry air advected over Kiruna creates a distinct snow virga regime.

The synoptic scale context associated with the precipitation events and the regimes also share similarities across the Scandinavian peninsula. Combined with the thermodynamic profiles of the atmosphere, the mean sea level pressure and geopotential height fields show how the large-scale circulation and types of weather events (such as extratropical cyclones and persistent cold air trapped in high pressure systems) influence the snowfall regimes.

This work also described potential mechanisms and processes involved in the development of snowfall during the precipitation events. The vertical profiles of temperature and relative humidity provided insight to potential riming, aggregation of particles and whether the conditions correspond to the dendritic growth zone. However, to further investigate and evaluate the processes and mechanisms taking place during the snowfall regimes, future work will include additional observations. At both sites, a NASA-supported video disdrometer called a Particle Imaging Package (PIP) was deployed. The PIP observes particle size distributions (PSDs), particle fall speeds and habit (Newmann et al., 2008). In Haukeliseter, a Multi-Angle-Snowflake Camera (MASC) recorded images of snowflakes to identify particle habit and size distributions as well. In Kiruna, colleagues at the Luleå University of Technology observe snowfall using a Dual - Ice Crystal Imager (D-ICI), which also takes high resolution images of naturally occurring snowflakes and ice

crystals. These additional measurements will provide a deeper look at the microphysics occurring in the development of the snowfall.

In addition to the microphysical properties of snowfall events, examining other products available in the ECMWF ERA5 reanalyses may provide further insight into these snowfall regimes. For some of the cases, especially the intermittent and intermittent/pulsed, the Integrated Water Vapor (IVW) could potentially link these events to extreme precipitation events such as atmospheric rivers. Sodemann and Stohl (2013) showed how atmospheric rivers impacting the Scandinavian coast persisted during multiple cyclones in December 2006. For the intermittent/pulsed snowfall case on 21 December 2016 in Haukeliseter, multiple cyclones brought intense precipitation to Scandinavian coast and mountains. How similar was December 2016 to December 2006?

While these snowfall regimes occur with some frequency during the winter months, the observations are limited to the two separate deployments and only one season per site. Additional deployments would be needed to evaluate whether those types of snowfall were specific to the years. For example, the entire month of December in 2016 was dominated by westerly winds at Haukeliseter, which implies that all of the events were intermittent/pulsed. But it is shown that the month was anomalously warm. Could the factors contributing to the surface temperature anomaly also be affecting the dominant winds? What other snowfall regimes exist on other parts of the Scandinavian peninsula or other regions in the high latitudes? Can they be characterized into the categories from Table 5.1? For example, coastal regions in Scandinavia experience Polar Lows; these

intense mesoscale storms readily form when Arctic cold air advects over the relatively warmer seas surrounding the peninsula (Noer et al., 2011). Do these Polar Lows generate a distinct snowfall profile? Or, can they also be organized into one of the categories from Table 5.1? Some questions regarding the atmospheric circulation and variability are also difficult to address from the scope of this project. Specifically, how might the North Atlantic Oscillation contribute to the regimes and surface temperatures? Longer periods of observations and space-based observations could help expand the study and answer these questions.

Bibliography

Bintanja, R. and O. Andry, 2017: Towards a rain-dominated arctic. *Nature Climate Change*, **7**, 263.

Collins, M., R. Knutti, J. Arblaster, J.-L. Dufresne, T. Fichefet, P. Friedlingstein, X. Gao, W. J. Gutowski, T. Johns, G. Krinner, et al., 2013: Long-term climate change: projections, commitments and irreversibility.

Devasthale, A. and L. Norin, 2014: The large-scale spatio-temporal variability of precipitation over sweden observed from the weather radar network. *Atmospheric Measurement Techniques*, **7**, 1605–1617.

Gisnås, K., B. Etzelmüller, C. Lussana, J. Hjort, A. B. K. Sannel, K. Isaksen, S. Westermann, P. Kuhry, H. H. Christiansen, A. Frampton, et al., 2017: Permafrost map for norway, sweden and finland. *Permafrost and Periglacial Processes*, **28**, 359–378.

Gorodetskaya, I., S. Kneifel, M. Maahn, K. Van Tricht, W. Thiery, J. Schween, A. Mangold, S. Crewell, and N. Van Lipzig, 2015: Cloud and precipitation properties from ground-based remote-sensing instruments in east antarctica. *Cryosphere*, **9**, 285–304.

Guan, B., N. P. Molotch, D. E. Waliser, E. J. Fetzer, and P. J. Neiman, 2010: Extreme snowfall events linked to atmospheric rivers and surface air temperature via satellite measurements. *Geophysical Research Letters*, **37**.

Hoskins, B. J. and K. I. Hodges, 2002: New perspectives on the northern hemisphere winter storm tracks. *Journal of the Atmospheric Sciences*, **59**, 1041–1061.

Houze Jr, R. A., 2014: *Cloud dynamics*, volume 104. Academic press.

Instanes, A., V. Kokorev, R. Janowicz, O. Bruland, K. Sand, and T. Prowse, 2016: Changes to freshwater systems affecting arctic infrastructure and natural resources. *Journal of Geophysical Research: Biogeosciences*, **121**, 567–585.

Kneifel, S., M. Maahn, G. Peters, and C. Simmer, 2011: Observation of snowfall with a low-power fm-cw k-band radar (micro rain radar). *Meteorology and Atmospheric Physics*, **113**, 75–87.

Kulie, M. S., L. Milani, N. B. Wood, S. A. Tushaus, R. Bennartz, and T. S. L’Ecuyer, 2016: A shallow cumuliform snowfall census using spaceborne radar. *Journal of Hydrometeorology*, **17**, 1261–1279.

Lamb, D. and J. Verlinde, 2011: *Physics and chemistry of clouds*. Cambridge University Press.

Libbrecht, K. G., 2005: The physics of snow crystals. *Reports on progress in physics*, **68**, 855.

Liu, J., J. A. Curry, H. Wang, M. Song, and R. M. Horton, 2012: Impact of declining arctic sea ice on winter snowfall. *Proceedings of the National Academy of Sciences*, **109**, 4074–4079.

Local, T., 2016: Norway’s december weather as warm as summer. *The Local*.

URL <https://www.thelocal.no/20161230/norways-december-weather-as-warm-as-summer>

Lund, M., C. Stiegler, J. Abermann, M. Citterio, B. U. Hansen, and D. van As, 2017: Spatiotemporal variability in surface energy balance across tundra, snow and ice in greenland. *Ambio*, **46**, 81–93.

Maahn, M. and P. Kollias, 2012: Improved micro rain radar snow measurements using doppler spectra post-processing. *Atmospheric Measurement Techniques*, **5**, 2661–2673.

Maahn, M., P. Kollias, S. Kneifel, I. Gorodetskaya, G. Peter, and C. Simmer, 2012: Measuring snowfall with a low-power k-band radar (micro raind radar) in polar regions. *ERAD 2012–The Seventh European Conference on Radar in Meteorology and Hydrology*.

Matrosov, S. Y., 2007: Modeling backscatter properties of snowfall at millimeter wavelengths. *Journal of the atmospheric sciences*, **64**, 1727–1736.

Matrosov, S. Y., M. D. Shupe, and I. V. Djalalova, 2008: Snowfall retrievals using millimeter-wavelength cloud radars. *Journal of Applied Meteorology and Climatology*, **47**, 769–777.

- Mitchell, D. L., R. Zhang, and R. L. Pitter, 1990: Mass-dimensional relationships for ice particles and the influence of riming on snowfall rates. *Journal of applied meteorology*, **29**, 153–163.
- Noer, G., Ø. Sætra, T. Lien, and Y. Gusdal, 2011: A climatological study of polar lows in the nordic seas. *Quarterly Journal of the Royal Meteorological Society*, **137**, 1762–1772.
- Norin, L., A. Devasthale, T. L’Ecuyer, N. Wood, and M. Smalley, 2015: Intercomparison of snowfall estimates derived from the cloudsat cloud profiling radar and the ground-based weather radar network over sweden. *Atmospheric Measurement Techniques*, **8**, 5009–5021.
- Norin, L., A. Devasthale, and T. S. L’Ecuyer, 2017: The sensitivity of snowfall to weather states over sweden. *Atmospheric Measurement Techniques*, **10**, 3249–3263.
- Perovich, D., T. Grenfell, B. Light, and P. Hobbs, 2002: Seasonal evolution of the albedo of multiyear arctic sea ice. *Journal of Geophysical Research: Oceans*, **107**, SHE–20.
- Pettersen, C., R. Bennartz, A. J. Merrelli, M. D. Shupe, D. D. Turner, and V. P. Walden, 2018: Precipitation regimes over central greenland inferred from 5 years of icecaps observations. *Atmospheric Chemistry & Physics*, **18**.
- Putkonen, J. and G. Roe, 2003: Rain-on-snow events impact soil temperatures and affect ungulate survival. *Geophysical Research Letters*, **30**.
- Rasmussen, R., B. Baker, J. Kochendorfer, T. Meyers, S. Landolt, A. P. Fischer, J. Black, J. M. Thériault, P. Kucera, D. Gochis, et al., 2012: How well are we measuring snow:

- The noaa/faa/ncar winter precipitation test bed. *Bulletin of the American Meteorological Society*, **93**, 811–829.
- Rinehart, R. E., 1991: *Radar for meteorologists*. University of North Dakota, Office of the President.
- Schirle, C. E., S. J. Cooper, M. A. Wolff, C. Pettersen, N. B. Wood, T. S. L’Ecuyer, T. Ilmo, and K. Nygård, 2019: Estimation of snowfall properties at a mountainous site in norway using combined radar and in-situ microphysical observations. *Journal of Applied Meteorology and Climatology*.
- Screen, J. A. and I. Simmonds, 2012: Declining summer snowfall in the arctic: Causes, impacts and feedbacks. *Climate dynamics*, **38**, 2243–2256.
- Seager, R., D. S. Battisti, J. Yin, N. Gordon, N. Naik, A. C. Clement, and M. A. Cane, 2002: Is the gulf stream responsible for europe’s mild winters? *Quarterly Journal of the Royal Meteorological Society: A journal of the atmospheric sciences, applied meteorology and physical oceanography*, **128**, 2563–2586.
- Serreze, M. C. and R. G. Barry, 2011: Processes and impacts of arctic amplification: A research synthesis. *Global and planetary change*, **77**, 85–96.
- Skofronick-Jackson, G., D. Hudak, W. Petersen, S. W. Nesbitt, V. Chandrasekar, S. Durden, K. J. Gleicher, G.-J. Huang, P. Joe, P. Kollias, et al., 2015: Global precipitation measurement cold season precipitation experiment (gcpex): for measurement’s sake, let it snow. *Bulletin of the American Meteorological Society*, **96**, 1719–1741.

Smalley, M., T. L'Ecuyer, M. Lebsock, and J. Haynes, 2014: A comparison of precipitation occurrence from the ncep stage iv qpe product and the cloudsat cloud profiling radar.

Journal of Hydrometeorology, **15**, 444–458.

Sodemann, H. and A. Stohl, 2013: Moisture origin and meridional transport in atmospheric rivers and their association with multiple cyclones. *Monthly weather review*, **141**, 2850–2868.

Souvereinjs, N., A. Gossart, I. V. Gorodetskaya, S. Lhermitte, A. Mangold, Q. Laffineur, A. Delcloo, and N. P. van Lipzig, 2018: How does the ice sheet surface mass balance relate to snowfall? insights from a ground-based precipitation radar in east antarctica. *The Cryosphere*, **12**, 1987–2003.

Souvereinjs, N., A. Gossart, S. Lhermitte, I. Gorodetskaya, S. Kneifel, M. Maahn, F. L. Bliven, and N. van Lipzig, 2017: Estimating radar reflectivity-snowfall rate relationships and their uncertainties over antarctica by combining disdrometer and radar observations. *Atmospheric research*, **196**, 211–223.

Stewart, I. T., 2009: Changes in snowpack and snowmelt runoff for key mountain regions. *Hydrological Processes: An International Journal*, **23**, 78–94.

Tatone, J., 2016: 'urd' has reached hurricane strength. *Norway Today*.

URL <https://norwaytoday.info/news/urd-reached-hurricane-strength/>

Vavrus, S., 2007: The role of terrestrial snow cover in the climate system. *Climate Dynamics*, **29**, 73–88.

- Vihma, T., J. Screen, M. Tjernström, B. Newton, X. Zhang, V. Popova, C. Deser, M. Holland, and T. Prowse, 2016: The atmospheric role in the arctic water cycle: A review on processes, past and future changes, and their impacts. *Journal of Geophysical Research: Biogeosciences*, **121**, 586–620.
- Vikhamar-Schuler, D., K. Isaksen, J. E. Haugen, H. Tømmervik, B. Luks, T. V. Schuler, and J. W. Bjerke, 2016: Changes in winter warming events in the nordic arctic region. *Journal of Climate*, **29**, 6223–6244.
- Ware, E. C., D. M. Schultz, H. E. Brooks, P. J. Roebber, and S. L. Bruening, 2006: Improving snowfall forecasting by accounting for the climatological variability of snow density. *Weather and forecasting*, **21**, 94–103.
- Wolff, M., K. Isaksen, A. Petersen-Øverleir, K. Ødemark, T. Reitan, and R. Brækkan, 2015: Derivation of a new continuous adjustment function for correcting wind-induced loss of solid precipitation: results of a norwegian field study. *Hydrology and Earth System Sciences*, **19**, 951–967.